DOKUZ EYLÜL UNIVERSITY

GRADUATE SCHOOL OF NATURAL AND APPLIED SCIENCES

FUZZY ENTROPY IN IMAGE PROCESSING METHODS FOR MEDICAL DATA

by

Yusuf YENİYAYLA

March, 2017

İZMİR

FUZZY ENTROPY IN IMAGE PROCESSING METHODS FOR MEDICAL DATA

A Thesis Submitted to
the Graduate School of Natural and Applied Sciences of Dokuz Eylül University
In Partial Fulfillment of the Requirements for the Degree of Doctor of Philosophy in Statistics Program

by
Yusuf YENİYAYLA

March, 2017
İZMİR

Ph. D. THESIS EXAMINATION RESULT FORM

We have read the thesis entitled **"FUZZY ENTROPY IN IMAGE PROCESSING METHODS FOR MEDICAL DATA"** completed by **YUSUF YENİYAYLA** under supervision of **ASSOC.PROF.DR. EMEL KURUOĞLU KANDEMİR** and we certify that in our opinion it is fully adequate, in scope and in quality, as a thesis for the degree of Doctor of Philosophy.

Assoc.Prof.Dr. Emel KURUOĞLU KANDEMİR

Supervisor

Prof. Dr. Efendi NASİBOĞLU

Thesis Committee Member

Prof. Dr. Oğuz DİCLE

Thesis Committee Member

Prof. Dr. Şaban Ören

Examining Committee Member

Doç. Dr. Hatice Özkoç

Examining Committee Member

Prof. Dr. Emine İlknur CÖCEN

Director
Graduate School of Natural and Applied Sciences

CHAPTER ONE
INTRODUCTION

This chapter contains three sections: an overview of the research and its objectives; a summary of the author's contributions and purpose and research question; and a guide to the structure of this thesis.

1.1 Overview

Thesis topic is to include methods to issues as fuzzy entropy, Magnetic Resonance Imaging (MRI) and motion artifact and using fuzzy entropy based on conjugate gradient method for motion artifact reduces in MRI. The aim at in this study is to develop a method of reducing the motion artifact in MRI images.

The technique of clinical diagnosis and treatment used in this study is one of the novel techniques MRI for patient health is efficient method. As a result of numerous discoveries discovered in the 1970s, this method has made important progress in the last 40 years. But, imaging technique has a sharp quality, which is usually even comparable to that of a digital image. MRI because of high resolution and contrast of soft tissue is used as a leading method in clinical trials. MRI images obtained from different sequences have in the culverts and high contrast resolution for common disease that is particularly preferred by doctors. Clearly MRI techniques have significantly superior imaging capabilities compared to CT, PET and X-ray techniques. MRI technique don't spread X-ray or radiation because of utilizes the high magnetic field due to rotation of the proton energy. This technique uses neither ionizing radiation nor radioactive materials. Thus, MRI techniques are preferred in terms of monitoring of the disease problems were created for human health. Because any known side effects that participation in voluntary associations of clinical trials is provided. Especially used easily in the study of neurology and psychiatry field. Neurology and clinical research as well as in applications with large MRI techniques in research and voluntary experiments is particularly preferred because it is harmless. MRI apparatus are particularly preferred due to the strong contrast qualities. Multiple

contrast ability has made an invention ground-breaking MRI technology of our time. Brain proton density in different tissues, depending on the physical flow and heat-imaging techniques like CT and MRI are inadequate according to the method. MR imaging because of some unsolved problems despite the incredible features is especially risky for patients who have metal type from the influence of high magnetic fields. Second, they are given in details in the fourth chapter as motion artifact. Motion distortions can be eliminated especially through raw data after image is obtained in prospective techniques such as CT and PET. As motion artifacts are seen as blurred and ghosting, they can create images which can't be accepted in terms of clinical analysis. Long scanning techniques which is used to obtain images having high resolution can be used to get MRI images apart from motion distortions made by limiting patients' conscious motion, such as breathing and rigid or non-rigid motion. MRI scan of the abdomen and thorax are challenging, because of this reason (Mesleh et al., 2003).

1.2 Purpose and Research Question

The problems related to control motion of the patient has many solutions. These are classic methods, such as physical constraints and sedation. These are specially designed with fast imaging techniques, as well as some sequences. However, this method has a number of disadvantages. Otherwise, there are some technological developments also increases the sensitivity of MRI increased resolution and motion. In this study, a better understanding of the transactions that occur in the MRI focuses on corruption would be more helpful for a solution. To test the proposed method and steps for improving image degradation is described in detail in this study. Three approaches used to prevent the motion, avoid from the effects of motion and correcting the effects of motion will be given in the other three chapters. In these chapters, specific techniques will be explained according to previous studies. Motion, Patient's conscious movement or physical movement due to cardiac activity or respiration causes distortion in MRI.

In this thesis, we propose a new motion artifact reduction approach, which is composed of fuzzy entropy, Magnetic Resonance Imaging (MRI) and motion artifact. The aim at in this study is to develop a method of reducing the motion artifact in MRI images. The new method are named as fuzzy entropy based on conjugate gradient (FECGM). The verbal or numerical expressions used in defining things, explaining events, giving order and in many other situations include fuzziness. For example, old, young, long, hot, cold, mild, cloudy, sunny and etc. Humans use these kinds of uncertain terms while explaining an event or taking decisions in particular situations (Klir & Yuan, 1995).

The measurement of fuzziness in fuzzy sets is an important step for practical fields. Entropy method is used to make goal-oriented calculations by manipulating data structures have become fuzziness. Fuzzy sets of the front should display shows that entropy is used in various scientific studies.

The concept of entropy in a closed container as a measure of an ideal gas of the disorder in the late 19th Century was introduced by Boltzmann. Information theory in the 1940's as the problems related to telecommunications has emerged as a method used in the solution. Under a very set by Shannon information theory seeks to explain the amount of information that exists within.

1.3 Thesis Organization

Evaluation of the research, the proposed method including description Fuzzy and Fuzzy Entropy based on conjugate gradient for motion artifact correction in medical data in MRI; this thesis consists of four parts as follows. Chapter 2 is described as a major method of fuzzy and fuzzy entropy method approaches. Chapter 3 represent introduction to the basic features of magnetic resonance imager. Chapter 4 in the expression of motion artifacts and related methods and their removal will be represented. Chapter 5 give a novel approach including fuzzy entropy based on conjugate gradient for the reconstruction and motion artifact reduce.

CHAPTER TWO
FUZZY ENTROPY

Fuzzy entropy and features as the basic method of the proposed approach in this section will be discussed. Usually there are uncertainties in the real universe. Fuzzy entropy is defined as a measure of fuzzy sets (Zadeh, 1965). Several authors have expressed the same thing as logically, despite using different definitions. In this thesis it is discussed how to adapt to different studies of this method.

Image is the projection of the fuzzy real world on the sensor. The clear, solid and special state of fuzziness and ambiguity is the Aristotle logic, thus fuzzy logic involves Aristotle logic. Human eyesight system can adapt easily to unknown in the data or knowledge. It is more appropriate to use more fuzzy expressions instead of accurate expressions in defining digitally the image properties, such as, what kind of a substance the object is, its colour or shape; or in designating where the corner of the object begins using grey pixel values, where the border of an fuzzy object is, and in which class the pixels belong. These problems can be solved via thresholding and classification processes on the image, asserting the commutative rules using insight or computations. Fuzzy entropy also use noise reduction in MRI (Kwan & Kwan, 2011).

The two principal component of the fuzzy system are fuzzy sets and the operations of these sets. Fuzzy logic designates rules over the fuzzy sets to the operators (Nasibov, 2008). Entropy is a well-known concept in thermodynamic physics used to measure the irregularity of a system. Entropy can also be used in measuring the amount of information that an event contains. The entropy computing types widely used in image processing are Shannon, norm and threshold methods. Shannon entropy is used in many areas of science and technology. In order to provide a quantitative measurement of the degree of uncertainty of uncertain variables is presented as the definition of uncertain entropy resulting from information deficiency. Entropy is one of the most widespread measurements of fuzziness. The purposed literature used methods is given below fuzzy entropy and generalized fuzzy entropy.

2.1 Definition of Fuzzy Entropy

Concept of fuzzy entropy is defined as a measure of fuzzy sets. Different authors have defined it in the way which seemed appropriate to them. In this thesis, we would like to question the property of the methods which was proposed. x_i, is definite as the greatest extent possible from set A with the measure of probability $P(x_i)$ and N is the number of A. Fuzzy entropy is represented in Eq. (2. 1),

$$H_{nonfuzzy}(A,P) = -\sum_{i=1}^{N} P(x_i)\log P(x_i) \tag{2.1}$$

where, $\sum_{i=1}^{N} P(x_i) = 1$ and $i = 1, 2, 3, \ldots, N$.

The subset "nonfuzzy" is applied to disconnect from the degree of fuzziness. As the amount of information in sets then entropy value also increases. We use the Lagrange multiplier method in Eq. (2.2).

$$F(A) = -\sum_{i=1}^{N} P(x_i)\ln P(x_i) + \lambda(\sum_{i=1}^{N} P(x_i) - 1) \tag{2.2}$$

The maximum of $H_{nonfuzzy}(A,P)$ obtained from in Eq. (2.3).

$$\frac{\partial F(A)}{\partial P(x_i)} = -\ln P(x_i) - 1 + \lambda = 0 \tag{2.3}$$

$P(x_i) = e^{\lambda - 1}$ for $i = 1,\ldots, N$ is obtained from Eq. (2.3). $H_{nonfuzzy}(A,P)$ attain the higher value, $P(x_1) = P(x_2) = \ldots = P(x_N) = \frac{1}{N}$ of set is represented as information set A exit

as possible with intensity. The histogram can be showed as a probability distribution as $P(x_i)$ in fact Eq. (2, 3) defined in ordinary domain.

2.2 Fuzzy Entropy Based on Shannon Function

μ is a membership level of fuzzy number x element of subset A in a universal *X*. The degree of membership value of an element x in the fuzzy set A is 0.5 and then entropy reaches the maximum. *F(X),* denotes fuzzy cluster defined on *X*. In contrast, *P(X)* shows the absolute or crisp cluster.

Complement operator *T(x) = 1-x* is expressed. This operator is commonly used in the literature (Fatemi, 2011).

The rules of the complementary operator T: $[0,1] \rightarrow [0,1]$ can be defined as:

1) $T(0) = 1$ and $T(1) = 0$,
2) if $\forall\, a, b \in [0,1];\ a \leq b$ then $T(a) \geq T(b)$,
3) T is presented as function of complementary operator,
4) $T\big(T(x)\big) = x$

The modifier operator given by Yager is given in Eq. (2.4) in case of 0<*u*<1.

$$T_r(x) = (1-x)^u \tag{2.4}$$

If *u*=1, Yager's complementary function to return the fuzzy entropy complementary operatory. Complementary operator of Yager, if $r \in (0,1)$, has only one cross over point $r = \frac{1}{\sqrt[u]{2}}$. The generalized fuzzy entropy function, $\Omega_r = F(x) \rightarrow R^+$ meets four conditions (Yager, 1995):

1) $\Omega_r(A) = 0$ and $A \in P(x)$.
2) $A = [r]$ then $\Omega(A)$ has the greatest value.

3) A^*, is a sharpening set, in case $\mu_A(x) \geq r$ it becomes $\mu_{A^*}(x) \geq \mu_A(x)$ and incase $\mu_A(x) \leq r$ it becomes $\mu_{A^*}(x) \leq \mu_A(x)$.

4) $\Omega_r(A^{T_r}) = \Omega_r(A)$, A^{T_r} is equal to complement of A.

A fuzzy set A of subset X, for example Kohen entropy function represented as Eq. (2.5), Kosko entropy function represented as Eq. (2.6), Tanimoto entropy function represented as Eq. (2.7) and Yager's entropy function represented as Eq. (2.8) are used in entropy measure (Kosko, 1994).

$$E(A) = \frac{M(A \cap A^{T_r})}{M(A \cup A^{T_r})} \tag{2.5}$$

$$E(A) = \sum_{i=1}^{N} \frac{\min(\mu_A(x_i), \mu_B(x_i))}{\max(\mu_A(x_i), \mu_B(x_i))} \tag{2.6}$$

$$E(A) = M(A \cap A^{T_r}) \tag{2.7}$$

$$E(A) = 1 - \frac{M(A \cup A^{T_r}) - M(A \cap A^{T_r})}{N} \tag{2.8}$$

where, it is defined as $M(A) = \sum_{i=1}^{N} \mu_A(x_i)$ and $i = 1,..., N$.

Shannon entropy, in the fuzzy entropy method, is given as the Shannon function. It is the most widely used entropy type used in the literature in image segmentation. Shannon entropy is computed in Eq. (2.9).

$$s(x) = -[x \ln x + (1 - x)\ln(1 - x)] \tag{2.9}$$

The generalized fuzzy entropy function based on fuzzy entropy defined as in Eq. (2.10).

$$E(A) = -\frac{1}{N \ln 2} \sum_{i=1}^{N} s(\mu_A(x_i)) \tag{2.10}$$

2.3 Fuzzy Entropy and Shannon Entropy for Image processing

R is the set of pixel values, $I_{xy}$is the grey value of point (x, y) of set R. The grey value of point (m, n) in R, is represented as $\mu_R(I_{xy})$ in fuzzy set in Eq. (2.11) (Forkert et al., 2011).

$$R = \{I_{xy}, \mu_R(I_{xy})\} \text{ and } 0 \le \mu_R(I_{xy}) \le 1. \tag{2.11}$$

The fuzzy cluster of the grey pixel value are obtained from the S-function defined as in Eq.(2.12).

$$S(x; a, b, c) = \begin{cases} 0, & x \le a \\ \frac{(x-a)^2}{(b-a)(c-a)}, & a < x \le b \\ 1 - \frac{X-c)^2}{(c-b)(c-a)}, & b < x < c \\ 1, & x \ge c \end{cases} \tag{2.12}$$

It defined as in Eq. (2, 12) the x values are obtained from grey pixel set. The shape parameters of S-functions are represented a, b and c. b value is located between a and c. Fuzzy entropy is the largest value when b value receives the value 0.5 (Forkert et al., 2011). Using fuzzy entropy method for the segmentation grey pixel value t is given in Eq. (2.13-2.14)

$$f(x,y) = \begin{cases} 0 & \mu(x,y) < T \\ 1 & \mu(\mathrm{x},\mathrm{y}) \ge \mathrm{T} \end{cases} \tag{2.13}$$

In this Eq. (2.13) if $\mu_R(t) = 0.5$ then T=t and T is the threshold value.

The thresholding method based on generalized fuzzy entropy is defined as m value using Yager's complement operator.

$$f(x,y)=\begin{cases}0 & \mu(x,y)\le T^{*}\\ 1 & \mu(\mathrm{x},\mathrm{y})\ge \mathrm{T}^{*}\end{cases} \tag{2.14}$$

In this Eq. (2.14), if $\mu_R(t)=r$ then T^{*}=t is the optimal thresholding pixel value. The modifier operator u=1 of complementary operatory of Yager for optimal segmentation is defined as $T(x)=1-x$.

When applying this method, Yager's complementary operator is used for generalized fuzzy entropy calculation. In image processing application using generalised fuzzy entropy based on t thresholding value is defined as in Eq. (2.15) (De Luca & Termini, 1988).

$$E(t)=-\sum_{i=0}^{t}\frac{p_i}{p(t)}\log_2\frac{p_i}{p(t)}-\sum_{i=t+1}^{L-1}\frac{p_i}{1-p(t)}\log_2\frac{p_i}{1-p(t)} \tag{2.15}$$

Here p_i value is defined as the probability of i. pixel value and $p(t)=\sum_{i=1}^{N-1}p_i$. The optimal thresholding t pixel value is available using the numerical approach defined in Eq. (2.16).

$$t=Arg\{\max(E(t))\} \tag{2.16}$$

An optimal t value obtained from inverse *E(t),* when *E(t)* value reaches maximum value. The optimal E (t) values are used in the application section of the thesis.

CHAPTER THREE
THE BASIC PRINCIPLES OF MAGNETIC RESONANCE IMAGING

In this chapter, we define of Magnetic Resonance Imager in terms of the laws of physics issues and consist of a motion-clinical image from this information. It will be discussed with the basic principles of magnetic resonance imager, described as mathematical model.

Magnetic Resonance (MR) phenomenon can be expressed accurately as the definition of quantum mechanics in nature, besides that it can be defined more accurately by means of classical physics such as 1.5 tesla showed in Figure 3.1. MR imaging is a radiation imaging method which has the highest resolving power analysing soft tissue contrast. Therefore, it is an imaging technique that a patient doesn't have to expose to ionizing radiation and that is used in the examination of all soft tissues in the body especially the nervous systems. It had been put into practise before the first practices of physical principles in 1924 Paul announced that some atomic cores have spin and magnetic moment characteristics and thus they turn back to their energy levels when they are exposed under the influence of a magnetic field. 1946: Bloch and Purcell proved that the nuclei in a strong magnetic field have absorbed electromagnetic radiation energy separating energy levels by the effect of magnetic field. 1952: Bloch and Purcell (physicist) shared the Nobel Prize. 1966: Ernst and Anderson, they implemented Fourier Transform techniques to NMR. Late 1960s: Waugh et al they have developed NMR imaging methods at the end of solid state NMR studies.1973: 2D image was taken by Lauterbur. 1980: Hawkens found out MR multiplanar imaging feature and revealed the first imaging lesions (Julian, 2008).

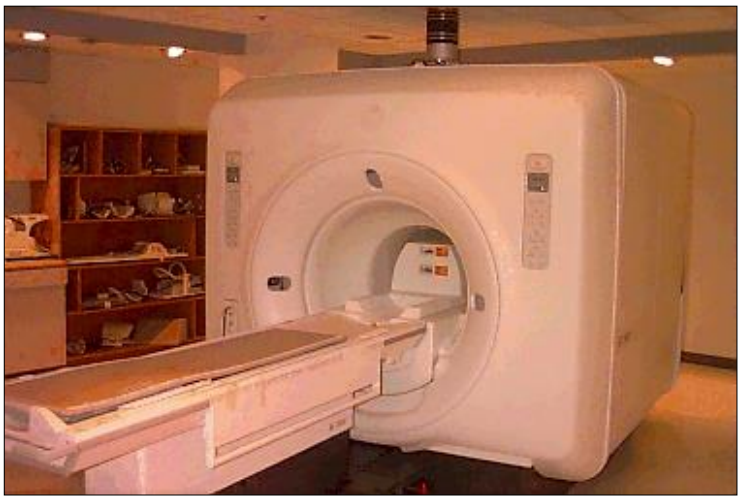

Figure 3.1 1.5 Tesla magnetic resonance imager MRI

MRI is a cross-sectional imaging techniques like CT (Amy et al., 2009). As in CT, imaging is formed by image processing methods by digitization values (Ryu et al, 2016). These digital images are processed utilizing computer technology and three-dimensional displays can be made. A major advantage of MR imaging is that it can also take images on each plane without changing the patient's position. Energy which MR uses are radio waves. The energy which is named as radiofrequency (RF), is located within the electromagnetic spectrum. Data source cytosolic and lipids wherein the hydrogen nuclei (protons).

Derivation of the MR image can be summarized as follows: Normally, our body is insensitive to RF energy. Firstly the protons which are our data source, should be turned into a position in which they can be stimulated by the RF energy. For this, the patient is placed in a strong magnetic field. Whit this magnetic pulse, protons are stacked in accordance with the magnetic field and they are turned into a position in which they can be stimulated. RF energy is delivered to the cross-section area. Protons take this energy and deviate from the position in relative with the amount of energy they took (Koharudin et al., 2003). RF-energy is cut. Protons return to their original position. During this turning process they emit out energy they receive as a signal form. By means of strong magnetic fields protons act like signal-emitting and signal-receding antennas. MR images are generated from these signals.

The meanings of grey tones of MR images vary according to the protocol inspection. But the white-light shades indicate increased signal areas and the dark-black shades indicate areas where there is little or no signal. Among the radiological methods MR is the method which show more detail in soft tissue. Due to displaying current, angiographic can be obtained without contrast agent.

3.1 Physics of MRI

The protons and neutrons which are basic structure of atomic nuclei rotate around their own axis. This is called spin movement. Due to their properties, protons behave like a magnetic bar and a magnetic field occurs naturally around their environment. Hydrogen atom have a strong magnetic field because its core consists of a single proton. This core which is abundant in the human body is ideal as the signal source (Madhu et al., 2003).

3.1.1 Basic Physics Principles and Bloch Equation

Normally protons are arranged randomly to eliminate the effects of each other in tissues (Michael et al., 2002). Thus, the body's magnetisation is zero in Figure 3.2.

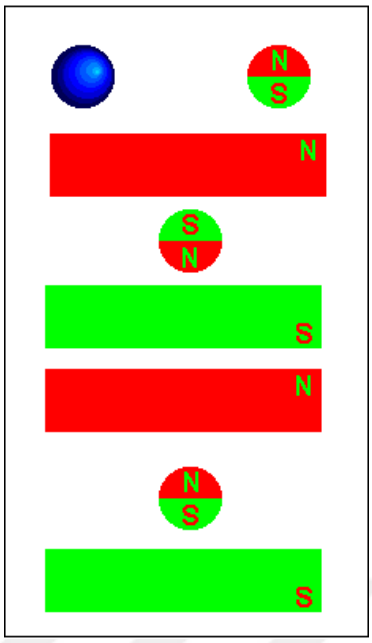

Figure 3.2 Spins and position in the magnetic field.

When the body part to be examined is located in a strong magnetic field, these protons pass parallel to the magnetic field vector like small iron rods behave in magnetic field. But this parallelism is not a static posture, it is with a rotation like a round the magnetic field. It turn is defined as precession. The frequency of precession of protons is ratio to the power of the magnetic field. Bloch equation in the absence of relaxation as defined in Eq. (3.1) (Flemming & Led., 2003),

$$\frac{\partial M}{\partial t} = M * \gamma B \tag{3.1}$$

where, * vector multiplication and gyromagnetic ratio γ MHz / T are given. The main magnetic field is B and net magnetisation vector is M, in the same direction. M and B are perpendicular to each other; it implies that the main magnetic field in the direction release required; this precession round the direction of the magnetic field. Precession rate, γ derived Eq. (3.1). In case of the failure of any magnetic field outside B_0 only component B is non-zero, the z-direction extends (Julian, 2008). z-direction magnetization given in Eq. (3.1) entirely clear in Eq.(3.2) expanded

$$\begin{pmatrix} \frac{\partial M_x}{\partial t} \\ \frac{\partial M_y}{\partial t} \\ \frac{\partial M_z}{\partial t} \end{pmatrix} = \gamma \begin{pmatrix} M_x \\ M_y \\ M_z \end{pmatrix} * \begin{pmatrix} 0 \\ 0 \\ B_z \end{pmatrix} \quad (3.2)$$

Evaluating the cross-product term gives,

$$\frac{\partial M_x}{\partial t} = \gamma M_y B_z$$
$$\frac{\partial M_y}{\partial t} = \gamma M_x B_z$$
$$\frac{\partial M_z}{\partial t} = 0 \quad (3.3)$$

re-creating Eq. (3.3) in terms of M_x and putting it into the case Eq.(3.4), it can be as shown below

$$\frac{\partial^2 M_x}{\partial t^2} = -\gamma^2 B_z^2 M_y \quad (3.4)$$

The solution given in the same terms in the equation of motion precession affected by magnetic fields and defines the harmonic movement represented in Figure 3.3.

$$\omega_0 = \gamma B_0 \quad (3.5)$$

Eq. (3.5) is defined as the Larmor equation in MRI.

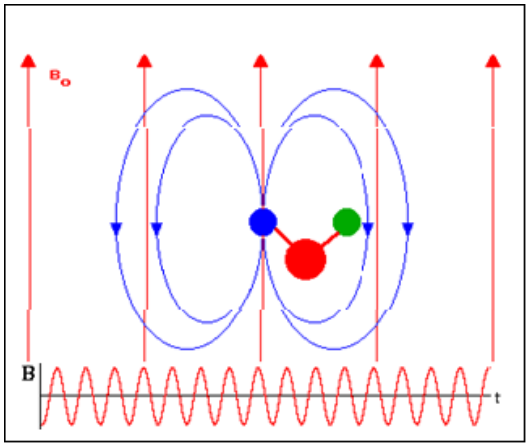

Figure 3.3 The magnetic field inside precession motion of spins,B_0 is the path of the magnetic field

Precession is the principle of magnetic resonance subject. To effect the protons, you need to make precession by putting them into magnetic field. But protons in this condition can come into resonance with RF in precession to be sent outside. Protons induced with radio waves make an angle by deviating from the position which is parallel to the magnetic field vector. When radio frequency (RF) is cut they return to their original position making precession. This is the MR signal we use to image alternating current produced by the movement of precession.

On the tissue in the magnetic field, spins in M_0 position is located within M_{xy} by the proper RF pulse. After the pulse is finished, spins likewise return by precession to M_0 position. The signal obtained from MRI scanners converted using Fourier Transformation for convolution or product them shown in Figure 3.4.

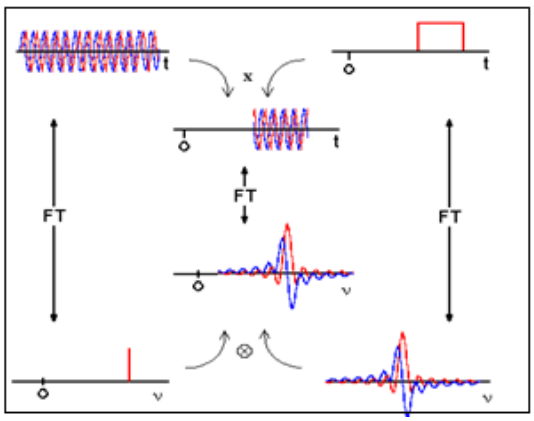

Figure 3.4 The magnetic field inside precession motion of Fourier transform

3.1.2 Obtaining the MR Signal

Let us put a phantom comprising water in a homogeneous magnetic field into the RF coil. Let us tie this RF coil to receiver and transmitter system by the help of a spanner. Let us place RF coil wrapped with phantom into the homogeneous magnetic field in a position in which the axis of symmetry is parallel with perpendicular magnetic field lines.

RF coils surrounding the phantoms containing water, the transmitter in a magnetic field of 1 Tesla magnitude if a signal having 42577 MHz frequency power is sent, and RF coil is moved to the receiver position immediately, it is appeared that RF signal decreases as an exponential function (Julian, 2008). This reducing signal is defined as the NMR signal. For water, in 1 tesla magnetic field, NMR signal can be observed only in the transmission frequency. This frequency is defined as the resonance frequency as M = 1 Tesla, f = 42 577 MHz and M = 2 Tesla, f = 85 154 MHz. Consequently, the intensity of the magnetic resonance frequency is rate with that of magnetic field.

When we do the same experiment with the phantom with different materials, we observed that each material doesn't produce NMR signals; different materials have different resonant frequencies under the same magnetic field strength as shown in Table 3.1 (Bourgeois et al., 2003).

The majority of the atoms, which are smallest particles of human body, have magnetic properties. Atoms consist of a core wrapped with one or more electron. The core consists of one or a more positive charged protons and neutral particles defined as neutrons. The core of the hydrogen atom only composed of a proton charged with positive. The advantages of hydrogen atom for the magnetic resonance:

a. It is the most common element found in the patient body,
b. It can be listed as the most sensitive elements in magnetic resonance.
Due to this characteristics, hydrogen protons are used in NMR imaging techniques.

Proton, neutrons and electrons have an important feature known as rotation around its axis. Each particle rotating around its own axis has magnetic properties. Rotating particles have also electric charge. Moving charges are defined as electric current. Electric magnetic field is altered by the time creates a magnetic field changing by the time. The opposite state is also valid. Looking at electromagnetic radiation, we can tell that precession surface of electric and magnetic field vectors are perpendicular to each other. In the NMR experiments, only the magnetic field vector (B_1) interacts with the object to be examined (Fagan et al., 2003).

Table 3.1 Basic Physics Principles - The electromagnetic spectra

Element	Biological Abundance*
Hydrogen (H)	0.63
Sodium (Na)	0.00041
Phosphorus (P)	0.0024
Carbon (C)	0.094
Oxygen (O)	0.26
Calcium (Ca)	0.0022
Nitrogen (N)	0.015

$$E = h\,V \tag{3.6}$$

where, E defines energy, h defines Planck's constant, f defines the frequency in Eq.(3.6) (Ernst et al., 2003).

Electric field causes electric current to occur in a conductive medium. This enables to occur magnetic field the around the conductor. On a straight conductor, the magnetic field lines around the conductor form a circular shape. If the conductor is a coil shape,

the total magnetic field of the coil is equal to the sum of each conductor of the magnetic field lines. But inside, the field lines are parallel. In a space without a magnetic effect, inside an ideal coil, a homogeneous magnetic field consists of. To measure the magnetic field, Tesla (T) is used as a unit: 1 Tesla = 10,000 Gauss. For checking, the value of the earth's natural magnetic field is about 0.5 Gauss value (Thomas, 2011).

Every material consists of atoms. Same or different atoms form molecules. Approximately 60% of the human body consists of water. The water molecules composed of an oxygen atom and two hydrogen atoms. The oxygen atoms in water molecules (H2O), is bound by a chemical bond, besides this the bound of carbon atoms in the fat molecules (CH-, CH2-, CH3-groups) is important also (Verdier et al., 2003) represented in Table 3.1. Therefore, the most abundant atoms in the human body are hydrogen atoms. But the hydrogen nucleus contains one proton (Bertram et al., 2003).

The core consists of protons and neutrons. The number of protons in the nucleus determines the chemical elements. Cores which have an equal number of protons but a different number of neutron are referred as isotope seeds. Cores have odd numbers of protons and /or neutrons, which have a measurable magnetic moment. As in a magnetic coil, magnetic field occurs rotation movement of electric charged particles. In space core may be perceived like a small ball rotating around its own axis. According to this model, the charged particles of core causes a circular movement due to rotation (Alonso & Massiot, 2003).

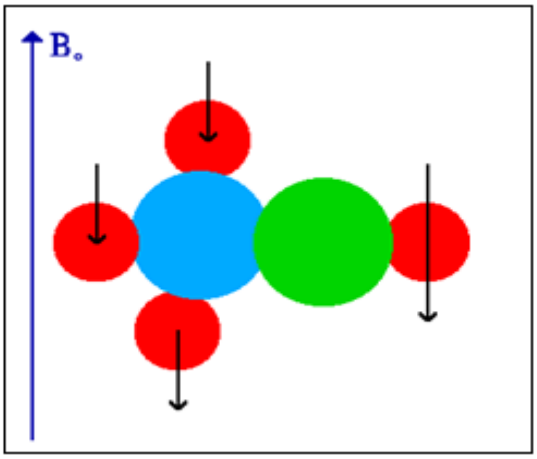

Figure 3.5 B_0 the position of the vector rotate in the non-direction magnetic field

The angular rotation momentum is defined as kernel. A proton has ½ level turn. In case of the absence of the magnetic field, rotating vectors of the hydrogen nuclei show randomly different directions. Therefore, the sum of rotating vectors doesn't bring about a net magnetic field measured on objects (Thomas, 2011).

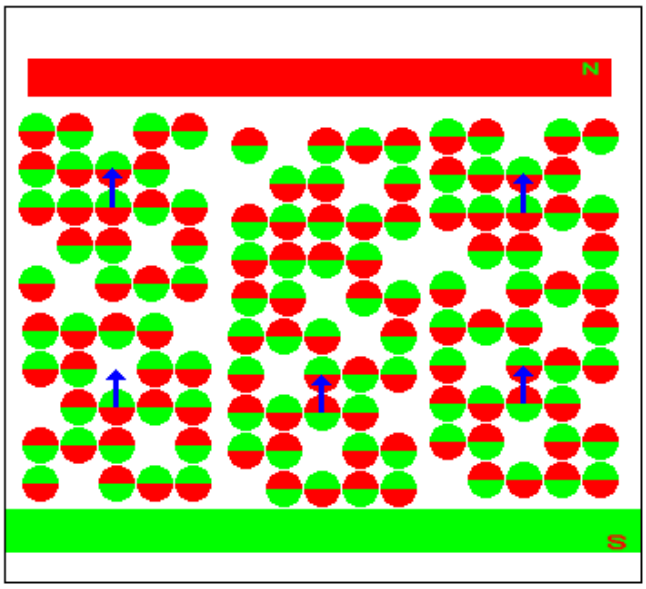

Figure 3.6 The position of the spin of the vector magnetic field

On a homogeneous magnetic field, rotation vectors of the hydrogen nuclei, i.e. proton may extend only same direction or antiparallel to the magnetic field as shown in Figure 3.6. Net magnetization direction as shown in Figure 3.5 will be the same provided that the numbers of protons extending parallel to the magnetic field are much more.

3.2 Energy Level of Protons

Back vectors of protons extending anti-parallel to the magnetic field have slightly higher energy level than that of protons extending parallel the magnetic field. Therefore protons need an energy which is proportional with the energy difference ΔE between two levels in Figure 3.7.

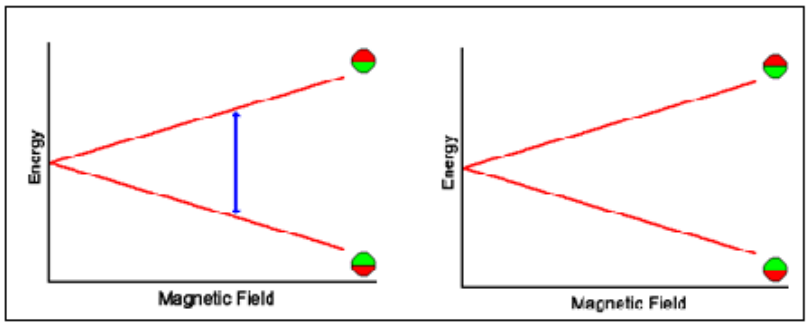

Figure 3.7 Energy level chart for parallel and non-parallel return vectors

The energy difference between (Δ) the two levels increase direct proportionally with the intensity of magnetic field. The number of protons extending same direction or antiparallel to the magnetic field is expressed by Boltzmann expression (Duer, 2002). Wherein the ratio of the protons in both cases, is related with the energy gap, thus related with applied magnetic field (B_0) in Eq. (3.6).

$$B_0 = kt \tag{3.6}$$

kt factor is a variable depending on the temperature. In this statement, k expresses the Boltzmann constant, t is the amount of thermal energy in Kelvin. In NMR studies temperature of the patient's body is fixed at 310°K. When the Boltzmann is examined, it can be observed that difference between the numbers of parallel or antiparallel protons is related the two levels 'energy difference thus is related with also B_0 magnetic area.

3.3 Larmor Frequence

It is possible experimentally to measure the parallel or antiparallel reflection value of the rotation vectors on the magnetic field vector. Components which are on the same direction and parallel to the magnetic field are defined "longitudinal" (longitudinal, likewise the ones which are right to the magnetic field is defined as "transversal" (cross). The cumulative effect of transversal components of the rotation vectors is negligible. Due to the magnetic momentum, protons move like quickly returning balls which are under the effect of the world's gravitation. Rotation vectors rotate about the

magnetic field axis at a frequency proportional with the B_0 magnetic field in the core field in Figure 3.8. Rotational frequency of rotation vector is defined as the Larmor frequency. In this phrase, proportional constant γ is defined as the gyromagnetic ratio and is a special value related with the size of the core. These values for the hydrogen atom are given as γ = 2.67522.

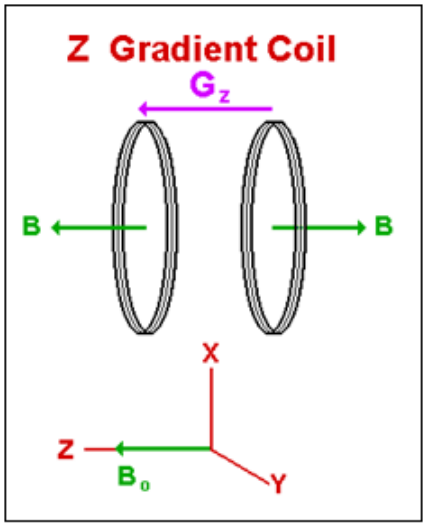

Figure 3.8 Larmor frequency of the rotation of the main magnetic field vector

Rotation vectors of protons in a 1 Tesla magnetic field vectors rotate at a 42,577 MHz frequency value. In NMR experiment, this frequency was particularly applied to a sample filled with water in of in order to obtain the characteristic MR signal. In NMR experiment the protons must be the same with the RF frequency transmitted by Larmor frequencies (Duer, 2002). The Larmor frequency and equation are named after the Irish Physicist and Mathematician Joseph Larmor (1857-1942). Firstly after the 90^0 slice selective pulse and slice selection gradient pulse applied and then phase encoding gradient pulse sequences and a frequency encoding gradient pulse sequences applied as given in Figure 3.9 and Figure 3.10.

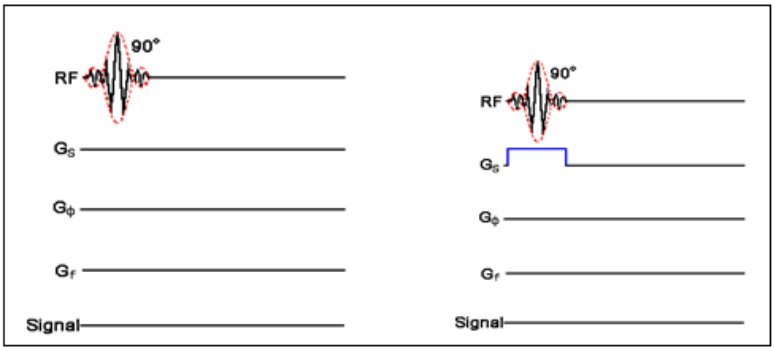

Figure 3.990[0] slice selective pulse and slice selection gradient pulse

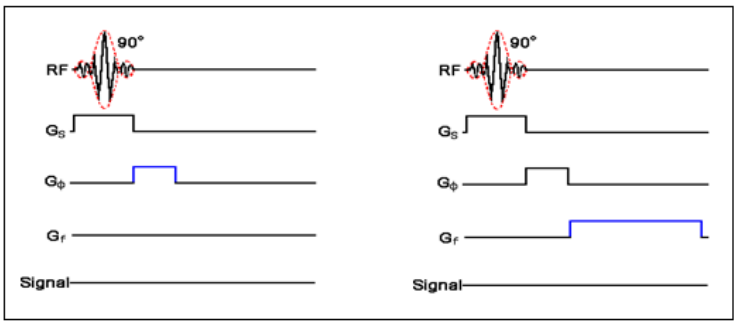

Figure 3.10 Phase encoding gradient pulse sequences and then frequency encoding gradient pulse sequences

If the transmitted RF frequency and (B_1 component) Larmor frequency (return to the rotation frequency of the vector) are associated with each other rotation vector of a proton moves from parallel position to he antiparallel position. At this stage, ΔE energy is drawn from the RF field. In the magnetic field, the phase angles rotation vectors aren't associated with each other. The MRI data obtained in this way are used in the application section of the thesis.

CHAPTER FOUR
MOTION ARTIFACT IN MRI

In this chapter, the problem of screening a mobile item will be discussed by emphasizing on general concepts given in literature. In the first part, the effects of patient's motion and the artifact occurred on the image as a result of motion of the item. Three approaches used to prevent the motion, avoid from the effects of motion and correcting the effects of motion will be given in the other three chapters. In these chapters, specific techniques will be explained according to previous studies. Motion; Patient's conscious movement or physical movement due to cardiac activity or respiration causes distortion in MRI.

These motion artifacts appear as problems also in other inspection methods, however, as inspection in MRI takes more time than other techniques, these artifacts becomes more distinctive.

4.1 Motion Artifact

In terms of understanding the analysis easily, the object which is about to be scanned is chosen to be a solid item only with rotational and reciprocating motions in accordance with obtained view in the direction of x and y coordination. During data acquisition, the motion of a view belonging to the body from reference point to a (x_0,y_0) point leads to bad data in phase encoding. Similarly, when the object is positioned according to reference as showed in the equation, phrase codding lines being in K-space are also positioned with the same direction and angle according to that.

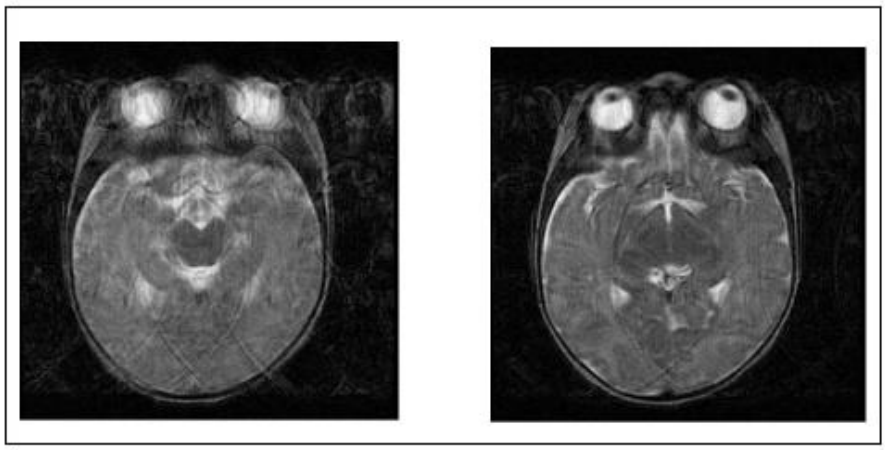

Figure 4.1The effected an axial head image of a patient (a) severe motion artifacts and (b) motion correction MRI image (Julian, 2008).

Since the motion is “freezed” for an effective time so that the distortion caused by motion will not be recorded as data acquisition in the direction of frequency encoding is quite fast. Due to this fact, existing discrepancies in k-space caused by the object motion occur only between the lines in the direction line of k-space. Discrepancies occurring in the direction of PE (Phase encoding) lead to shading and ghosting in the image in the same direction blurring (Figure. 4.1) (Julian, 2008). Ghosting which is described as the repetition of blurred image or a part of it is known to be caused by point spread function(PSF) having a broad peak. Ghosting is made by more common oscillatory of PSF (Reeder et al., 1997).

4.2 The Effects of Patient’s Movement

Raw data acquisition time in magnetic resonance imaging changes based on special sequences which used for k-space gathering. It is understood from MRI researches that the risk of patient’s movement is high while the image of the patient through MRI is acquired and it may take some time. Types of motion may affect the image acquisition negatively (Scott et al, 2009):

• Large scale/ bulk motion: The motion of the whole item which can be described as a patient’s head or body motion.

• Respiration: The motion caused by the patient’s breathing.

• Cardiac Motion: The motion of cardiac muscle or a large blood vessel.

• Blood Flow: motion of blood through a different stable slice.
• Gastrointestinal peristalsis: The motion of intestine and what is inside due to peristalsis.

Respiratory motion can be prevented by holding breath technique. (Knutsson et al., 2016) However, in case of scanning taking long time, counting the period of breath or respiratory organised phase encoding direction (ROPE) technique is used. Furthermore, the issue of cardiac motion is usually decreased by the technique of cardiac gating. The effects of blood flow can be decreased by using techniques for example gradient field reduces.

These techniques above have been used for years: These researches are briefly available in the article of Bellon and his friends in 1986. Bulk motion is still an important problem in MRI. In the method recommended, bulk motion in one single acquisition sequence will be shown. It is emphasized that there isn't any motion between sequences; this problem can be solved by the second image recording techniques. A simple experiment is made to measure head motion while the patient tries to stay stable like a healthy person (Knutsson et al., 2016).

4.3 Motion Prevention

The best approach to avoid from the most distinctive and used MRI motion is preventing the motion of an object. At least one of the techniques described here should be used for a detailed research.
The most distinctive and commonly used method to prevent image distortion considerably is restricting the motion of the object. At least one three of the techniques given here should be used to make the most effective clinical diagnosis. This techniques are called Physical Restrictions, Sedation and Training respectively.

4.3.1 Physical Restrictions

A head inside of the coil is tried to keep stable by using foam pillow and bean bags: The patient is nearly always immobilised by using a physical restriction in MRI. It is aimed to give the least disturbance by using these techniques; however, stabilising obtained is usually not enough. There are many other types of physical restrictions. Bite blocks are sometimes used; this object which has the shape of custom ray is asked to be held from patients during scanning. This technique can considerably decrease the motion. On the other hand, personalized restriction techniques create disadvantage as they lead discomfort. In addition, an object given to the mouth of a patient may increase the risk of deglutition as it leads to head motion. Edward and the others have successful results stated in the report in which a plaster head holder is used (Julian, 2008). It is stated that they are quite successful and the device is better in terms of patient tolerance when they are compared with braking slings which have low levels of rotational and reciprocating motions. It is stated that in contrast to some systems, the patient can always go out from the scanner device, which makes the decrease of the patient's anxiety possible. The main disadvantage is the time spent for tuning and preparing of every necessary equipment during the night and the cost. For this reason, this system is not accepted as clinic even though it is probably useful for his research.

4.3.2 Sedation

This method situation of the subject is acceptable sometimes to prevent motion during MRI. There are various disadvantages for the patient having sedation. An anaesthetist may be required as patients having sedation are exposed to some complications during scanning. Even though it is common in clinical usage, it is not used for research volunteers due to security concerns. For example, it is known that children have the risk of sedation hypoxia during MRI and CT scans (Scott et al., 2009). In addition, Potential functional MR (fMRI) is not used due to sedation problem.

4.3.3 Training

Patient training is possible to keep themselves immobilized during scanning. Even though it takes time, a decrease in repetition of scanning due to scan time can be obtained. Scanning process is stopped when the head motion of subjects exceeds the limit during video track. The decrease in this limit has proved that this is an effective technique of immobilizing. This approach is accepted as suitable for healthy individuals while it is not for patients having acute diseases (Keith et al., 2002).

4.4 Motion Effects Avoidance

Some techniques used for MRI have fewer tendencies to motion distortion comparing to the other techniques. In terms of image quality and resolution, of course, it costs time. If the predicted movement of patients can change their browser settings by operator. After obtaining the data or at the stage of obtaining data can be corrected motion artifacts. These methods are defined as retro prospective or prospective the process operation, which these technique are fast imaging and radial imaging.

4.4.1 Fast Imaging

If MRI data acquisition was fast enough for a simple chest x-ray, the motion of patients wouldn't create a problem. However, the system of MRI is extremely slow. On the other hand, there are many ways to decrease the image reception. The successful comparison of these techniques is stated by Slifer. As a trade-off occurs in the process between image reception and image quality, this comparison is normally quite useful. By this way, an image obtained causes significant decrease in image quality even though it is not affected by motion artifact. The fast spin echo (FSE) which was firstly defined by Hennig and his colleagues, is the technique in which 'conventional spin echo sequences' only an echo is produced per by an excitation pulse with 90 degree while less distorted images are produced. Basically, only in TR process, k-space decreases the scanning period by taking more than a line (Slifer et al., 1993).

The number of echoes during FSE sequence in MRI process is also defined as echo train length (Netl). Netlim pulse with 180 degrees which comes after every pulse with 90 degrees is generally called as a shot. A shot limits the number of lines obtained per process in k-space due to signal decrease affecting T2. In the practice, this number may barely exceed 32 lines (Julian, 2008). If the number of lines obtained in TR process is 32, this standard significantly decreases imaging period comparing to a spin echo sequence.

4.4.2 Radial imaging

Using an obtained radial k-space is more possible than obtaining data directly in k-space on a Cartesian Coordination system. This kind of data acquisition is more sensitive against disruptions caused by motion than Cartesian techniques (Pandit et al., 2010). Data acquisition in Spiral imaging in Figure 4.2 starts at the centre of k-space and spreads outwards slowly. Successful solutions are obtained by using fMRI spirals. In addition, it is not required for acquired raw data at one time in MRI, that is, it might be added between. Radial imaging can also be used as 3D (Jackson, et al., 1992). For instance, Shu and the others proved it's their trajectory activity in 'Under sampled Spherical Shells'.

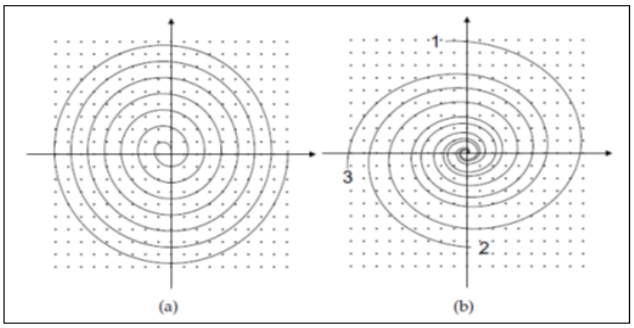

Figure 4.2 Two radial acquisitions sequences: (a) one trial-shot and (b) three trial-shots.

Some significant problems affect radial data acquisition. Even though these problems are decreased, off-resonance ghosting is one of these effects (Kirsten et al., 2001). Also, radial techniques oversampled in the centre of k-space may be disadvantageous in terms of image quality when sampling time is taken short. What's

more, data should be gridded to reproduce the image by using FFT when a Cartesian trajectory which does not exist is used (Julian et al., 2008).

4.5 Motion correction

The third approach can be practiced by motion artifact firstly occurring to avoid from motion artifact, measurement of it, eliminating or correcting it. Some techniques to correct it are tested and used in clinics (Pandit et al., 2010). These kinds of techniques usually include sequence designing and post-processing together. Sequence designing techniques can be expressed as navigator echoes, propeller, motion tracking and correction and post-processing techniques.

4.5.1 Navigator Echoes

The ones who firstly mentioned Navigator echo were Lehman and Felmlee in 1989. Since that time, navigator echoes have been commonly used among research groups, but they have not been used for clinical scanners to correct the head motion. However, it is usually used for cardiac motion artifact. Including basic practice of this technique, a data in k-space is repeatedly copied while data is sampled during acquiring of k-space data left. Navigator shows information about the motion of an object after post-processing. The data collected during motion can be eliminated depending on distortion hypothesis. This system is not very efficient; all data might be eliminated in cases of too many motions (Julian, 2008).

4.5.2 Propeller

One of the motion correction methods is PROPPELLER (Periodically Overlapping Parallel Lines with Enhanced Reconstruction) technique for MRI (Ahunbay & Pipe, 2000). Tis technique is later shown in clinic researches and simulations that it is effective in decrease of motion (for a T2 weighted imaging in the beginning) (Pipe, 1999, 2000). The original practicing explanation of PROPELLER technique of Pipe is given briefly here.

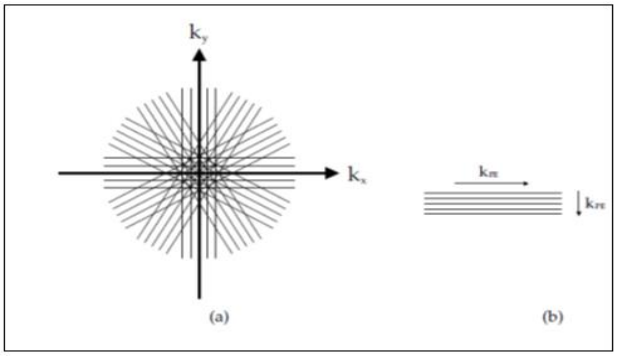

Figure 4.3Weighted average of all strips are used in correlation approach as a function of all correlation rotation angle

The next step is rotation corruption. Weighted average of all strips are used in correlation approach as a function of all correlation rotation angle (James, 1999). Angle of rotation of given strip is taken for peak value by adding quadratic polynomial function. These stairs in k-space are rotated and placed on the right coordination in Figure 4.3 (Julian, 2008).

4.5.3 Motion Tracking and Correction

Some outer cameras can be used for observing patients' motions and correcting data during data processing step. Lots of successful systems are practiced. Some other systems are required for retrospective correction and motion observation by using external monitoring system and detected motion correction after data processing data processing (Hinge-Chiu et al., 2013). Real time motion correction has another benefit. Screening is used during motion scanning of an object and scanner slopes act according to the motion of object by using its own data. By using this scanner, data is acquired through six parameter data which symbolizes the position in 3-D space and its orientation. Specific post-processing techniques are required this (Julian, 2008).

In the beginning of the year 1999, laser detection device was used for subject motion and three laser and three solid-state position detectors were used for having images without motion artifact. Every laser was placed to be sensible against reflectors which were placed on the skull of the subject. The slope of medical camera was

decided according to the subject's skull position after the angle of reflection was used. It is claimed to have positive results in this case, however, any experimental data or image can't be generalized by a single result.

4.5.4 Post-Processing Techniques

Various mathematical approaches by Sarty et al were claimed to correct motion effects occurred after data acquisition. But, these kinds of pulse sequences techniques are normally quite limited (Sarty, 2000). A free reference image may sometimes be required while a motion may be limited with one-dimensional and there might be some inconsistencies during practicing of simplification or hypothesis. Another technique is Autofocus which was firstly stated by Atkinson and his colleagues. According to this theory, entropy in the image finds rotational and reciprocating values minimizing the focus criteria so that motion artifacts can be decreased by using the most suitable figuration (Gonzales & Woods, 2008). The results showed that there is a significant correction in motion artifact effects. It is combined with a similar technique called parallel screening.

Another technique has recently published by Batchelor, Atkinson and their colleagues. Motion distortion is modelled by using a matrix equation system. It is stated that this technique creates a distorted image from the point of an ideal version. Here, after the process, a distorted version belonging to data turns into an ideal image which is identified before (Sarty, 2000). The inverse of the matrix equations using MATLAB which is the opposite of matrix equation is made by using LSQR routine practice (conjugate gradient is used). The cost function should be made to find the most accurate value which is converged by algorithm and evaluate images (entropy is used again). Researchers claim that the most disadvantageous part of this approach is the length of calculation time (Julian, 2008). Converge of the matrix system to a solution element is seen as a possible problem. In addition, motion parameters should have a high level of limitation. Techniques discussed above have the advantage of making any necessary changes in most cases. The results till now are more promising than the other techniques given in this chapter.

In this dissertation, we suggest a new technique depending on post processing. Motion of a patient when data acquisition affects artifacts on rotation and reciprocating images which occur on k-space line. Displacements caused by rotation and reciprocating can be eliminated by using a conjugated gradient approach depending on fuzzy entropy management (Julian, 2008).

CHAPTER FIVE
APPLICATION

Motion of patients leads to distortion of images during MRI scanning. Different techniques have been improved to eliminate these distortions. These techniques used during acquisition are called prospective techniques. They are given in details in the fourth chapter. Plug-in software is required during the practice of retrescopic techniques. Motion distortions can be eliminated especially through raw data after image is obtained in prospective techniques (Zahneisen et al., 2016).

Patient motion during MRI scanning may lead to severe distortions in image quality. As motion artifacts are seen as blurred and ghosting, they can create images which can't be accepted in terms of clinical analysis. Long scanning techniques which is used to obtain images having high resolution can be used to get MRI images apart from motion distortions made by limiting patients' conscious motion. Automatic focusing symbolizes techniques.

Even though motion correction has a wide literature, a universal solution of the problem does still not exist. Existing techniques can be divided into two groups as prospective and retrospective techniques. Free motion artifact images can be obtained by coordinating pose monitoring magnetic field based on patient's motion through outer sensors such as continuous monitoring. After the image is totally obtained, it is possible to eliminate motion distortions by retrescopic techniques (Bourgeois et al., 2003). After the calculation of correlation of adjacent lines in k-space with entropy approaches, recoding of k-space is made by estimation of point spread function through transfer. To estimate this subject motion, parameters of rotation and translation occurring related to adjacent k-space lines are firstly calculated using new method as fuzzy entropy based on conjugate gradient method (FECGM). In addition, this technique based on navigation and coding of obtained data are recorded in k-space to measure the motion.

In terms of image quality, it is proven that they can compete with navigator based techniques according to clinical researches. FECGM techniques mainly depend on researches to solve image denonising and problems in deblurring. FECGM is may use for motion balancing in radar ranging located in frequency area (Angelina et al., 2012). In the recent years, 3D screening systems have been improved to corrupt complicated motions including rotations occurring in FECGM techniques in MRI. Recently, retrospective approaches are suggested for correction of the whole rigid body motion, however, reference data are needed as the number of unknown motion parameters is high (navigator based monitors).

In this thesis, we suggest a retrescopic technique based on gradient entropy. An area including motion distortion in k-space and data to corrupt in this area depend on the calculation of the most optimal cost function (Wenda et al., 2005). In the suggested technique, phase coding which is 6 free parameters per step is used to obtain 3D images with high resolution (Ravindranathan et al., 2003). Whether there is a difference in the direction of phase coding or frequency coding due to motion in near trajectories can be estimated by taking a trajectory thought to have no distortion as a base. With the suggested methods of fuzzy entropy based on conjugate gradient method FECGM, translation and rotation parameters can be estimated. K-space will be reorganized with parameter values which make the cost function minimum based on the technique between every phase encoding line and adjacent lines in k-space. It is observed that the algorithm motion correcting based gradient is more efficient than the others in terms of time efficiency. It is quite hard to find the initial trajectory, namely phase encoding line, which especially is not affected from motion distortion. In addition, taking estimated entropy per parameter in the whole k-space as minimum with this technique is an optimal approach for image quality.

There are some inefficient techniques which only optimize the local distortions made by the estimation of some forward parameters. Analytical gradient techniques are suggested in the literature for the execution of some optimization operation. The provable convergence parameter and making parameter space can be made by coarse to fine strategy (Lauze et al., 2015). Interesting enough, degraded derivative based

optimization can be possible for making image quality with objective view efficient exploration. It can be calculated by using fast Fourier translation whose hypothesis degree isn't single uniformed (Bourgeois et al., 2003). Assume that in the other approaches, similarly, recurrence time TR is taken longer to model the dynamic orbit as a time of starting scaled piecewise constant function (Wenda et al., 2005).

In this chapter, firstly, modelling of how raw data is affected by motion distortion in k-space will be mentioned. Then, Fuzzy entropy cost function based on conjugate gradient metric will be organized. After this process, multi-scaled optimization will be used in calculation of translation and rotation parameters to minimize objective function. Following section, with the estimated parameters in the corrected k-space MRI image it describes how to create re-organized. Quality metrics for the evaluation of results obtained using the most commonly used methods in the literature. Performance of the Motion Correction methods is defined as Signal to Noise (SNR), Normalized Root Mean Squared Error (NRMSE) and Difference in Background Energy (DBE). Process for collecting data, and then results obtained by using this method will be shown.

5.1 Motion Correction Model

MR scanners obtain Fourier coefficient multiples along with sharp trajectories as dictated by MRI gradient patterns. Optimization transactions will be made by taking k-space (raw data) obtained line-by-line as basis in Figure 5.1.

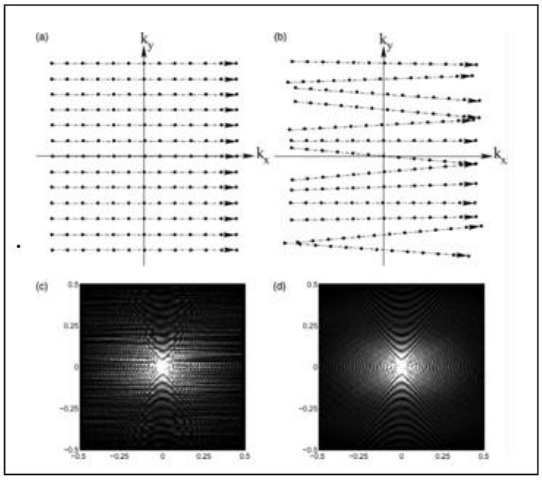

Figure 5.1 (a) Cartesian coordinates of k-space (b) rotation translation corrupted by motion of k-space. (c) Shepp–Logan experiment phantom (d) k-space after reconstruction of the rotation and translation corrupted by motion artifact in k-Space.

*R*aw data of corrupted image matrix $I \in C^{n_x \times n_y}$is converted to column vector $I \in C^N$ of size$N = n_x n_y$ in Eq. (5, 1).

$$I = \begin{bmatrix} I_{11} I_{12} \dots I_{1x} \\ . \\ . \\ . \\ I_{y1} I_{y2} \dots I_{yx} \end{bmatrix} and\ I = \begin{bmatrix} I_{11} \\ I_{21} \\ . \\ . \\ I_{yx} \end{bmatrix} \tag{5.1}$$

where, fourier matrix $F \in C^{NxN}$, M_t is partial of k-space and M_t=$diag(m_t)$, m_t=$\{0,1\}^N$ masking coefficients at time t, $TR(a_t)$ represent rigid motion transformation matrix, $a_t$denote motion and translation parameters. a_t composed of two translation and one rotation parameters and$a_t \in R^{3T} x[0,2\pi)^{3T}$ at any time t. M_t containing the section of k-space which is filled by a MRI sequences at same time t. Finally sharp image $I_t$obtained from provided Eq. (5.2) (Se Young, 2009).

$$I_t = \int_0^T M_t TR(a_t) F dt I \tag{5.2}$$

Cartesian MR measurements are two specific time frame. One of them echo time TE another repetition time TR in MRI data acquisition. Lines of k-space settings are

defined in the best way by representing the length of each TR is T repetitions sequence (Fellner et al., 2010). We assume that the subject moves during the re-conversion of the rigid matrix, (a_t) changes minimal. Thus, integral can be estimated by measuring total and masking, it would have been closer together in Eq. (5.3). The total number of discrete integral form Eq. (5.3) is converted to the form given Eq. (5.2) (Se Young, 2009). Thus, represented in Eq. (5.2), which also form the integral sum of the discrete number will return the form provided Eq. (5.3) (Bourgeois et al., 2003).

$$I_t = \sum_{t=1}^{T} diag(m_t)TR(a_t)FI \tag{5.3}$$

5.1.1 Translation and Rotation Parameters

We use that raw data in MRI lines including a dimension of size $n_x n_y n_z$ pixels are obtained, hence T = $n_y n_z$ repetitions are requested for 3D imager and T = n_y for 2D imager. Each repetition, a motion correction of $diag(m_t)TR(a_t)FI \in C^N$ is obtained. The m_t is a binary mask contains n_x nonzero components $[TR(a_t)]FI \in C^{n_x}$ is showed Eq. (5.4) where the shortcut $[TR(a_t)] \in C^{n_y xN}$. Finally, we can put all motion parameters into a single matrix of $TR(a) = \sum_{t=1}^{T} diag(m_t)TR(a_t)$ which consisting of blocks of size n_x.

$$I_t = TR(a)FI, \tag{5.4}$$

Rotation parameter space and translation space are presented in Eq. (5.5)

$$R(a_t) = \begin{bmatrix} Ra_1 & 0 & 0 & 0 & 0 & \dots & 0 \\ 0 & Ra_1 & 0 & 0 & 0 & \dots & 0 \\ 0 & 0 & Ra_1 & 0 & 0 & \dots & 0 \\ & & & \dots & & & \\ 0 & 0 & 0 & \dots & Ra_2 & 0 & \dots 0 \\ & & & \dots & & & \\ 0 & 0 & 0 & 0 & 0 & \dots & Ra_T \end{bmatrix} \in C^{NxN}, T(a_t) = \begin{bmatrix} Ta_1 & 0 & 0 & 0 & 0 & \dots & 0 \\ 0 & Ta_1 & 0 & 0 & 0 & \dots & 0 \\ 0 & 0 & Ta_1 & 0 & 0 & \dots & 0 \\ & & & \dots & & & \\ 0 & 0 & 0 & \dots & Ta_2 & 0 & \dots 0 \\ & & & \dots & & & \\ 0 & 0 & 0 & 0 & 0 & \dots & Ta_T \end{bmatrix} \in C^{NxN}, \tag{5.5}$$

where,$I_t \in C^{NxN}$ is parameterized by $a = [a_1, a_2, \dots, a_T] \in R^{3T}x[0,2\pi)^{3T}$composed of translation and rotation, the matrix including the parameters of raw(k-space) data and $T = n_x n_z$ for 3D imager and T = n_y for 2D imager.

Rotation parameter space $R(a_t)$ includes θ_t rotation angle made in the counter clockwise direction obtained by iterative techniques of synchronous phase encoding line for every line in k-space. Corrected new k-space is obtained by multiplication of every line in I_t space which also means k-space with Ra_ttransformation matrix Eq. (5. 6).

$$Ra_t = \begin{bmatrix} cos\theta_t & -sin\theta_t \\ sin\theta_t & cos\theta_t \end{bmatrix} \tag{5.6}$$

$TR(a_t) = R(a_t)x\, T(a_t)$, $TR(a_t)$composed of blocking matrix[$TR(a_t)$]size n_x each and $TR(a_t)$ finite difference matrix in Eq. (5.7) (Callaghan et al., 2015).

$$TR(a_t) = \begin{bmatrix} TR(a_1) \\ TR(a_2) \\ . \\ . \\ . \\ TR(a_T) \end{bmatrix} \tag{5.7}$$

5.1.2 Forward Model for Motion Correction

Forward dynamics model estimates future condition of input data. Similarly, the future values of late MR signals can be estimated by Forward dynamics model. As feedback time of sensors takes long, it is significant to use Forward model to make faster correction. Motion matrix which is $TR(a_t)$ codded includes parameters related to motions such as coil sensitivity. *I* artifact-free image and final $I_t$image is showed in Eq. (5.8) (Yingying & Connor, 2015). Least squares solution: We have purposed 'Conjugate gradient techniques based on fuzzy entropy such as LSQR' methods for solving above forward model using in Eq. (5.8).

$$min \quad \|TR(a_t)I - I_t\| \tag{5.8}$$

$$I_t = M_t TR(a_t) FI \tag{5.9}$$

$$\begin{bmatrix} I_1 \\ I_2 \\ . \\ . \\ . \\ I_N \end{bmatrix} = \begin{bmatrix} m_1 & 0 & 0 & 0 & 0 & \dots & 0 \\ 0 & m_2 & 0 & 0 & 0 & \dots & 0 \\ 0 & 0 & 0 & 0 & 0 & \dots & 0 \\ & & & \dots & & & \\ 0 & 0 & 0 & m_t & 0 & \dots & 0 \\ & & & \dots & & & \\ 0 & 0 & 0 & 0 & 0 & \dots & m_N \end{bmatrix} \begin{bmatrix} TRa_1 & 0 & 0 & 0 & 0 & \dots & 0 \\ 0 & TRa_1 & 0 & 0 & 0 & \dots & 0 \\ 0 & 0 & TRa_1 & 0 & 0 & \dots & 0 \\ & & & \dots & & & \\ 0 & 0 & 0 & \dots & TRa_2 & 0 \dots & 0 \\ & & & \dots & & & \\ 0 & 0 & 0 & 0 & 0 & \dots & TRa_T \end{bmatrix} \begin{bmatrix} 1 & 1 & 1 \dots 1 \\ 1 & w & w^2 \dots w^{n-1} \\ 1 & w^2 & w^3 \dots w^n \\ & & \dots \\ & & \\ & & \dots \\ 1 & w^{n-1} & w^n \dots w^{(n-1)^2} \end{bmatrix} \begin{bmatrix} I_{11} \\ I_{21} \\ . \\ . \\ . \\ I_{NN} \end{bmatrix} \tag{5.10}$$

M_t part of k-space, I_t acquisition part of k-space of raw data, $N = n_x n_y$ in 2-D or N= $n_x . n_y . n_z$ in 3-D and $T = n_y n_z$ lengt of repetition time in TR or phase encoding lines in k-space (Shu et al., 2006). I image transformation at current shot, TR (a_t) multiplication of image by coil sensitivity map *F* Fast Fourier Transform to k-space for selection of acquired k-space for current shot. I_t=$M_t TR(a_t)FI$ equation composed of Eq. (5.9) and Eq. (5.10) is solved using Eq. (5.8) (Michael, 2015).

5.1.3 Fuzzification of Spatial Domain

Fuzzyfication is the process of transforming k-space values between L_{min} and L_{max} into (0,1) fuzzy numbers. Here, ramp function is used for transforming fuzzy values in Eq. (5.11).

$$\mu(I_t) = \frac{I_t}{L_{max}} \tag{5.11}$$

Algorithm: Parameters calculation of S-Shaped function. Assume the input image $\mu(I_t)$ has grey level range between $L_{min}$to L_{max}. Detailed procedure of calculation a, b, c and parameters are as follows: To calculate S-Shaped function's parameters, input screen having grey pixel pitch between L_{min} and L_{max} is given $\mu(I_t)$ (Pushpa et al., 2015).The shape of S-function is determined by parameter a, b and c. The parameters obtained as $a = L_{min}$, $b = L_{max}$ and $c = (L_{min} + L_{max})/2$.

For motion correction, fuzzy entropy modification is performed. Here we used S-Shaped membership function for the motion correction in MRI. The S-shaped functions have three parameters of input and give the altered membership plane or properties plane (Alexander, 2003). The S-shaped membership function is presented in Eq. (5.12) with using S-Shaped membership function the shape of the input image $\mu(I_t)$.

$$\mu^*(I_t) = S(\mu(I_t), a, b, c) = \begin{cases} 0 & \mu(I_t) \le a \\ \frac{(\mu(I_t)-a)^2}{(b-a)(c-a)} & a < \mu(I_t) < b \\ 1 - \frac{(\mu(I_t)-a)^2}{(c-b)(c-a)} & b \le \mu(I_t) < c \\ 1 & \mu(I_t) \ge c \end{cases} \quad (5.12)$$

5.1.4 Cost Function

Our goal is to estimate the parameters of motion in degraded image and then corrected them. We take into account the model including translation and rotation consisting of small angle may also it can be invertible (Srinivasa et al., 2012). Experimental approach as the inverse to take (a_t) parameter matrix applied to the corrupted image *I (*Dung et al., 2009*)*. We are interested in (a_t)parameters of the cost function to optimize clear medical image using the minimization of parameters.$D_x$and $D_y$horizontal and veritical finite differences matrices in Eq.(5.13) (Pushpa et al., 2015).

$$H(I_t) = H^*(D_x I_t) + H^*\left(D_y I_t\right) \quad (5.13)$$

$H^*\left(\mu^*(I_t)\right)$ is a gradient entropy using fuzzy entropy based on conjugate gradient method (FECGM), $\mu^*(I_t) \odot \overline{\mu^*(I_t)}$ pointwise (Hadamard) product and $\mu^*(I_t)^H \mu^*(I_t)$matrix product in Eq.(5.14). $\mu^*(I_t)$ is the fuzzy membership function of $I_t$and $\mu^*(I_t)^H$ conjugate transpose of $\mu^*(I_t)$in Eq.(5.12).

$$v = \sqrt{\left(\frac{\mu^*(I_t) \odot \overline{\mu^*(I_t)}}{\mu^*(I_t)^H \mu^*(I_t)}\right)} \in R^{Nx1} \quad (5.14)$$

$$H^*(Dv) = -(Dv)^T \ln(Dv) \in R^+ \quad (5.15)$$

$a_t = argmin\left(H\left(\mu(I_t)\right)\right)$ composed of translation $T_a$and rotation parametersR_a. γ is a trajectory of a correction parameter that controls the smoothness. D is a finite

difference matrix in Eq.(5.16) and cost function is minimized using chain rule including FECGM in Eq.(5.17) (Allison, 2016).

$$a_t = argmin\left(H\left(\mu(I_t)\right)\right) + \gamma\|Da_t\|^2, \tag{5.16}$$

$\frac{\partial TR(a_t)I}{\partial(\mu(I_t))} = TR(a_t)'I$ is contain all information needed for matrix derivative

$\frac{\partial TR(a_t)I}{\partial a_t^T} = diag(TR(a_t)'I)$, which is diagonal matrix because of each row depend on a_t.

$\frac{\partial\left(H(\mu(I_t))\right)}{\partial a_t^T}$ denote derivative Jacobian matrix of by mean of chain rule and then we represent in Eq.(5.17) (Kim et al., 2008).

$$\frac{\partial\left(H\left(\mu(I_t)\right)\right)}{\partial a_t^T} = \frac{\partial\left(H\left(\mu(I_t)\right)\right)}{\partial\left(\mu(I_t)\right)}\frac{\partial\left(\mu(I_t)\right)}{\partial a_t^T} \tag{5.17}$$

5.1.5 Translation and Rotation Properties in K-space

The transformation of scanned objects affects phase encodings in k-space negatively. Phase encoding straights in k-space will change place if the object is transferred from a reference point to another (x_0, y_0),

$$f(x,y) \Leftrightarrow ₣(k_x, k_y)$$

$$f(x_0, y_0) \Leftrightarrow ₣\left(k_x, k_y\right)exp(-i2\pi\left(k_x x_0 + k_y y_0\right)) \tag{5.18}$$

where, $\Leftrightarrow$ show the Fourier transforming in Eq. (5.18) which is known as the two-dimension Fourier shift theorem (Abaci et al., 2015).

It is also a useful technique for analysing the effect of a rotating subject in view on k-space. When an image, for example, on an (x, y) point is turned its image center according to a new coordination (x_0, y_0) with a related angle, the new k-space is given here in Eq. (5.19) (Pandey & Noll, 2006).

$$\begin{bmatrix} x_0 \\ y_0 \end{bmatrix} = \begin{bmatrix} cos\theta & -sin\theta \\ sin\theta & cos\theta \end{bmatrix} \begin{bmatrix} x \\ y \end{bmatrix} \tag{5.19}$$

$$f(xcos\theta - ysin\theta, xsin\theta + ycos\theta) \leftrightarrow \mathbb{F}(k_x cos\theta - k_y sin\theta, k_x sin\theta + k_y cos\theta) \tag{5.20}$$

The same angle at which the object rotates in the back of k-space data as indicated Eq. (5.20).

5.2 Parameters Estimation

The next step after building novel motion artifact correction model and data obtaining is the prediction of translation and rotation parameters. This section, the purpose is to specification the translation and rotation parameters of the subject from k-space. This problem is solved using magnitude of raw data by Eq. (5.9-5.10). Translation and rotation parameters estimation respectively can be described below.

5.2.1 Translation Parameters Estimation

$I_t: R^2 x R^+ \rightarrow R$ denote an image MRI sequence in k-space and w=(b,c,t) is the translocation parameter, which amount the windows at time *t* and the windows at time *t+1*. Chiefly of the appearing motion improvement algorithms begin with the k-space magnitude level invariance assumption that is the value of the k-space magnitude doesn't change while moving in Eq. (5.21):

$$I_t(x_1 + b, x_2 + c, t + 1) = I_t(x_1, x_2, t) \tag{5.21}$$

More exactly, using coarse to fine to predict *w* of the subject motion parameter at a supplied the k-space magnitude location $p = (x_1, x_2, t)$, one approaches for an update, $\mu(I_t) = I_t$ and$dw = (db, dc, 0)$, for example,

$$I_t(p + w + dw) = I_t(X) \tag{5.22}$$

The linearization of the above in Eq. (5.22) meet the expressed as shifted OFC equation in Eq. (5.23).

$$dw\nabla^w I_t = 0 \tag{5.23}$$

where, $\nabla^w I_t$ is the shifted or motion compensated gradient and matrix form showed in Eq.(5.24)

$$\nabla^w I_t = \begin{bmatrix} \frac{\partial I_t(p+w)}{\partial x_1} \\ \frac{\partial I_t(p+w)}{\partial x_2} \\ I_t(p + w) - I_t(p) \end{bmatrix} \tag{5.24}$$

This method represent how to application these in a ‘‘multiscale coarse-to-fine method’’. Assumption stable *dw* update an exponential neighbourhood of *p*, we use a method of RMSE at *p* truly as in Eq. (5.25). The growing domain dw is expressed at each point of k-space as the minimisation of the quadratic energy is defined below

$$E_w(dw) = dw^T S^w dw \tag{5.25}$$

where, $S^w = (\nabla^w I_t)(\nabla^w I_t)^T$ is a shifted or motion artifact which ‘‘compensated structure tensor’’. Minimisation of the quadratic energy given in Eq. (5.23) is solved by using the following algorithm (Wang et al., 2005).

1. Set $w^{N+1} = 0$
2. for *n=N, N-1,…1, 0*

* Equation the shifted structure tensor $S^{w^{n+1}}(X) = h_k\left(\nabla^{w^{n+1}} I_t\right)\left(\nabla^{w^{n+1}} I_t\right)^T$

* Computing the bring up to date dw^n defined as the minimum value of the quadratic energy implies that $E_{w^{n+1}}(dw)$.

* $w^n = w^{n+1} + dw^n$

3. Output w^0 (h_k denote the spatio-temporal Gaussian kernel).

5.2.2 Rotation Parameters Estimation

We are interested in minimizing the quadratic function $\Omega: R^N \to R$ given by

$$\Omega(x) = \frac{1}{2}x^T Ax - x^T b \tag{5.26}$$

The minimum value of w= (b, c, t) is obtained by setting the gradient equal to zero.

$$\nabla\Omega(x) = Ax - b \tag{5.27}$$

Linear equation, Ax=b and discover the solution by using r =b−Ax and $A\theta = H(I_t)$ parameterized $\theta = [\theta_1, \theta_2, \ldots, \theta_T]$ (Kim, 2008). The parameters of rotation that is using in Eq. (5.26) into Eq. (5.27) and then Eq. (5.26) is obtained from Eq. (2.28).

$$\nabla\Omega(\theta) = A\theta - b \tag{5.28}$$

$$\theta_{k+1} = \theta_k + \alpha_k p_k \tag{5.29}$$

a_k and p_k parameters updated by using the above mentioned direct method and iterative methods and then θ_k are generated, p_k is a vector, α is a scalar as search direction determines the direction of steps length. In general we find the exact solution in at most n iterations. Convergence speed depends on the square root of the condition in Eq. (5.29). Start with some θ_0=0.

Set $p_0 = r_0 = b - A\theta_0$ and for k=0, 1, 2, 3, …

$\theta_{k+1} = \theta_k + \alpha_k p_k, \ \ \alpha_k = \frac{r_k^T r_k}{p_k^T A p_k}$

$r_{k+1} = b - A\theta_{k+1} = r_k - \alpha_k A p_k$

$p_{k+1} = r_{k+1} + \beta_k p_k, \ \ \beta_k = \frac{r_{k+1}^T r_{k+1}}{r_k^T r_k}$

$r_n = 0\ exact\ solution$ and find optimal rotation parameters θ_{k+1}.

5.3 Motion Correction and Image Reconstruction

A practice including 3T components of translation and rotation process is made for reorganizing at operators. To make translation correction, every line phase ramp in k-space $\exp(-2\pi i k_x a_t)$ a transfer function of spatial domain t distorted by multiplying of image let us obtain Fourier multipliers k_x (Nan-kuei & Alice, 2004). It is necessary to look how $TR(a_t)I$ block matrix is made of at parameters to understand Matrix multiplying better. Firstly, $(a_t)I$ block matrix is divided into translation and rotation parts and every translation part is multiplied spatially with local phase shift and the transfer grid of rotation part $R \in R^{NxN}$Cartesian grid $g \in R^{3xN}$ is resampled (resampling) and on transferred Cartesian grid k$\in R^{Tx1}$. Gridding matrix W_{ij} in Eq.(5.30) which is made again is showed.

$$TR(a_t)I = T(WI) \tag{5.30}$$

* Translation of x- (frequencies encoding) direction in Eq. (5.31),

$$t_x = \exp(-2\pi i k_x b_i)\ and\ \ \frac{\partial}{\partial t_\theta} t_x\ = -2\pi i b_i * t_x \tag{5.31}$$

* Translation of y- (phase encoding) direction in Eq. (5.32),

$$t_y = \exp\left(-2\pi i k_y c_i\right) and\ \ \frac{\partial}{\partial t_\theta} t_y\ = -2\pi i c_i * t_y \tag{5.32}$$

Rotated grid vectors $k^i \in R^{1x1}$are attained from Cartesian grid lines by a localised rotation $R^i g^i$ as optained by a rotation motion parameter matrix $R^i \in R^{1x1}$depending on one rotation parameter (Chaumette et al., 2003). Input values of gridding matrix is obtained from the function application window. Renewed k-space grid parameter k_j and the before Cartesian location parameterg_i, such that in Eq. (5.33) (Nan-kuei & Alice, 2004).

$$G_{ij} = w\left(k^i{}_x - g^i{}_x\right) w\left(k^i{}_y - g^i{}_y\right) \tag{5.33}$$

Other representation for example Euler angles are too large. Put in everything together, we obtain the following translate parameters *x, y, z*-direction to grid on renewed Cartesian grid.

$\frac{\partial}{\partial t_x} TR(a_t)I = t_x{}' t_y t_z(GI)$ translate x-direction grid on new cartesian

$\frac{\partial}{\partial t_y} TR(a_t)I = t_y{}' t_x t_z(GI)$ translate y-direction grid on new cartesian

$\frac{\partial}{\partial t_z} TR(a_t)I = t_z{}' t_y t_x(GI)$ translate z-direction grid on new cartesian

$\frac{\partial}{\partial \theta} TR(a_t)I = T(W'I)k_\theta{}'$ rotation clockwise centred k-space grid on new Cartesian

5.4 Performance of the Motion Correction

The measure of how degraded by a picture for the reason motion is an important concept corruption. (For example, such offered by Pipe) Other correction algorithms often on the test reporting is based on the post-image processing. (Pipe, 1999) is based on the visual appearance instead. Although not denying the importance of the evaluation of the images for clinical benefit provides an objective metric algorithm that measured the effects of subtle changes. There are several important considerations in the development of metrics for comparing an image correction movement experiments. These methods given as Signal to Noise (SNR), Normalized Root Mean Square Error (NRMSE) and Difference in Background Energy (DBE) respectively.

5.4.1 Signal to Noise Ratio (SNR)

Statistic range of motion parameters whose stimulation is made is suitable for the range of standard error of rotation σ_θ and a Gaussian range whose standard error is pixel. As a result, different signal-to-noise ratios $SNRI$ are found by adding complex image Gaussian noise as showed in Eq. (5.34) (Yuusuke, et al., 2016).

$$SNR_I = \frac{\frac{1}{N}\sum_{n=0}^{N-1} I(n)}{\sigma_{noise}} \tag{5.34}$$

The number of pixels in N Object I is taken as N. By defining SNR value in k-space as in pixel space, algorithm is made to give more optimal results. When more high frequency is placed in k-space for Cartesian sampled data, SNR value will be found higher than edges. Generally, the signal on every trajectory is defined with its SNR value. SNR_k and motion parameters are evaluated as a equation of SNR_k. This equation is also given in j. trajectory in Eq. (5.35) (Kim et al., 2008).

$$SNR_k = \frac{\frac{1}{N}\sum_{n=0}^{N-1} k_j(n)}{\sigma_{noise}} \tag{5.35}$$

5.4.2 Normalized Root Mean Squared Error (NRMSE)

The number of trajectory samples are N and standard error of Gaussian noises σ_{noise}. To improve the performance of motion correction, suitable criterions based on NRMSE will be chosen from the object as it is shown in Eq. (5.36) (Ahunbay & Pipe, 2000),

$$NRMSE_{object} = \frac{1}{\sqrt{\sigma_{I_{art}}^2 + \sigma_I^2}} \sqrt{\frac{\sum\left(I_{art} - I_{cor}\right)^2}{N_{object}} - \left(\frac{\sum\left(I_{art} - I_{cor}\right)}{N_{object}}\right)^2} \tag{5.36}$$

where, I_{art} corrupted(degraded) image is compared with I_{cor} corrected(reconstruction) image, the number of pixels in the object is given as N_{object}. Standard error of NRMSE noise is normalized. With this technique, in case of $NRMSE_{object}(I)$ value being 1, it can be concluded that two images have the same feature, which means noise is eliminated. The success of the algorithm is given with the reduction rate R_{NRMSE} Eq. (5.37) in which is measured by the elimination of artifact (Yuusuke et al., 2016),

$$R_{NRMSE} = 100\frac{NRMSE_{object}(I_{art}) - NRMSE_{object}(I_{cor})}{NRMSE_{object}(I_{art}) - 1} \tag{5.37}$$

where, I_{art} and I_{corr} are the images before and after motion correction, respectively. In case of totally elimination of the artifact in the image, R_{NRMSE}=100% will be obtained (Yuusuke et al., 2016).

5.4.3 Difference in Background Energy (DBE)

Pixel density of the region outside the field-of-view (FOV) is expected to be zero in an MRI image. But pixel density can be seen in this area due to motion artifact. It is expected to decrease after this intensity reduced movement distortion. This movement changes the amount of decrease may indicate the success of the process of reducing distortion.

The total energy of corrupted (degraded) image ($T_{corrupted}$) and the total energy of corrected (reconstruction) images ($T_{corrected}$). The background energy for each images ($B_{corrupted}$ and $B_{corrected}$). The equation is computing by Eq. (5.38):

$$DBE = \frac{B_{corrupted}}{T_{corrupted}} - \frac{B_{corrected}}{T_{corrected}} \tag{5.38}$$

5.4.3 Evaluation of radiologists

Observations of radiologists are of clinical significance in the evaluation of medical images. The results obtained from the images in terms of diagnosis are evaluated by the radiographs of the naked eye. Radiologists are asked to rate the corrupted image and the corrected image to see if there is any improvement. The scores obtained are analyzed by t-test and the results are evaluated.

5.5 Data Acquisition and Applications

This section details of applications with the sequence information and parameters of data obtained from MRI scanners the will be described.

5.5.1 Data Acquisition

3T Siemens MRI scanners having birdcage coil feature are used in screening tests in Figure 5.2. It is observed during the screening process that the object which is designed for well-defined 2D motion (2 transition 1 rotation DOF) placed of MR-adaptable holder is successful in motion parameter control in 2-D screening. Raw data is obtained from UMRAM in Bilkent University use our study for purposed our method performance.



Figure 5.2 Siemens MAGNETOM Trio system with 8-channel transmitter series which placed UMRAM is also open on the use of researchers

Within the framework of local ethics, firstly one human brain images are obtained. After the subject placed his head as to stay stable, it is asked to move his head in a direction. With standard screening protocols, neuroscience research sequence and parameters are used for 2-D images in this research. Multi-slice RARE sequence is used for 2-D imager. Per each echo train, 8 echoes are used and 4 slices with 4 mm diameters are obtained. In total, these slices and the images got from FOV of 400×160 mm2 and encoding with a matrix size of 384×160 and 40 ms TE and 2.5 seconds TR time took 75 seconds.

In addition, monkey brain and kiwi fruit images with 1024×666 matrix over a FOV of 440×286 mm2 is obtained with a high quality from other from other experiment in http://mloss.org/software/view/430/.

5.5.2 Applications and Evaluation of Results

The proposed FECGM algorithm is used for gradually more strong motion correction processes given next section. After algorithm optimization parameters with data whose 2-D simulations are made, transactions on real data are performed.

To provide a distorted data, we perform transactions on 2-D image which do not have a motion distortion with the forward model made for data creation by us (Yingying & Connor, 2015). The results (reconstruction image) are compared with the corrupted image while our own reconstruction algorithm is compared with certain reference values (Peder et al., 2008). Motion trajectory is made in sinusoidal form for each motion parameter.

Sinus motion form is chosen for the conformity of analysis of motion trajectories obtained for real reference value. For instance, the analysis results of recovered trajectories as it is seen in Figure 5.3. All motion parameters are obtained in sine-form by using an out-of-phase for 2D image (192x192) related to brain. All the 100 successful attempts with random initial values showed optimizer algorithm success. The results from all attempts are given with sine-form graphics with their original and corrected images.

How much translation and rotation parameters departed from their original location can be observed when the normal sine-form graphic is compared with sine-form graphics of experimental results. It is seen that low and medium frequency ranges give quite successful results in the estimation of motion parameters as they are less affected by the motion.

Seven raw data including motion artifact analysed by proposed method results are shown in Figure 5.3-5.9. The results are discussed in the success of the proposed algorithm by comparing the quality metric methods.

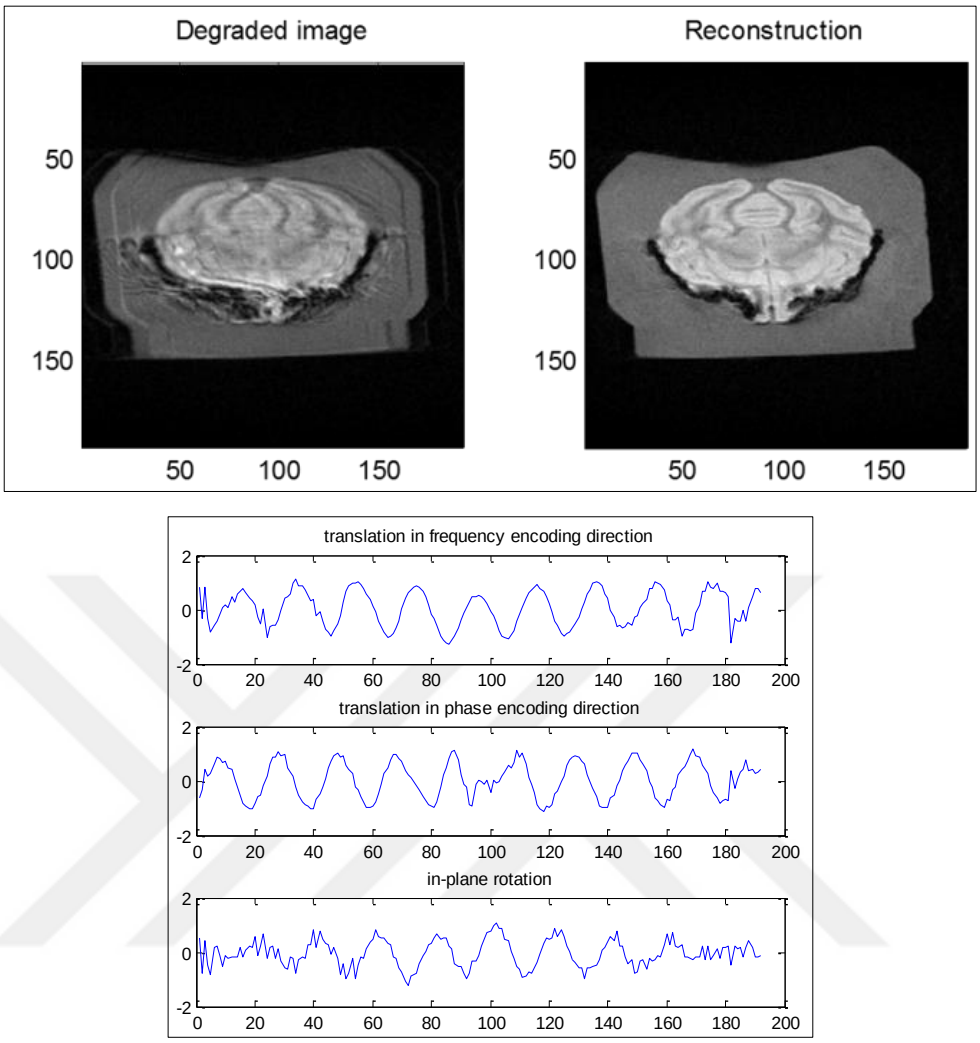

Figure 5.3 Monkey brain image with 2D dimension (raw data1). Left: degraded image of monkey brain. Right: corrected with using optimization of image quality metric over the raw data. The bottom chart, with random values launching three DOFs algorithm parameters are obtained in 2D: Depends on the straight line trajectory shows a sinusoidal curve motion.

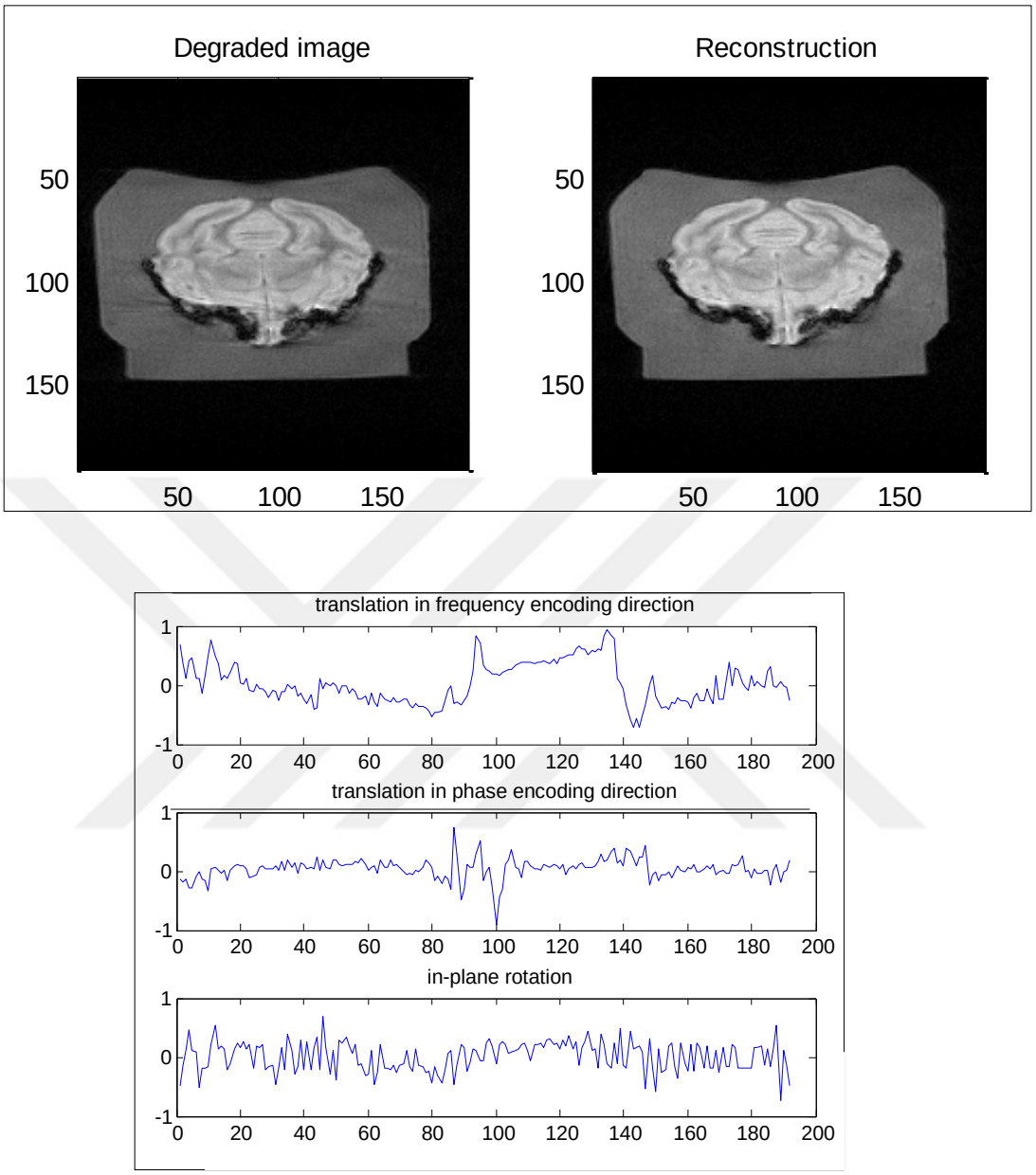

Figure 5.4 Monkey brain image with 2D dimension (raw data 2). Left: degraded image of monkey brain. Right: corrected with using optimization of image quality metric over the raw data. The bottom chart, with random values launching three DOFs algorithm parameters are obtained in 2D: Depends on the straight line trajectory shows a sinusoidal curve motion.

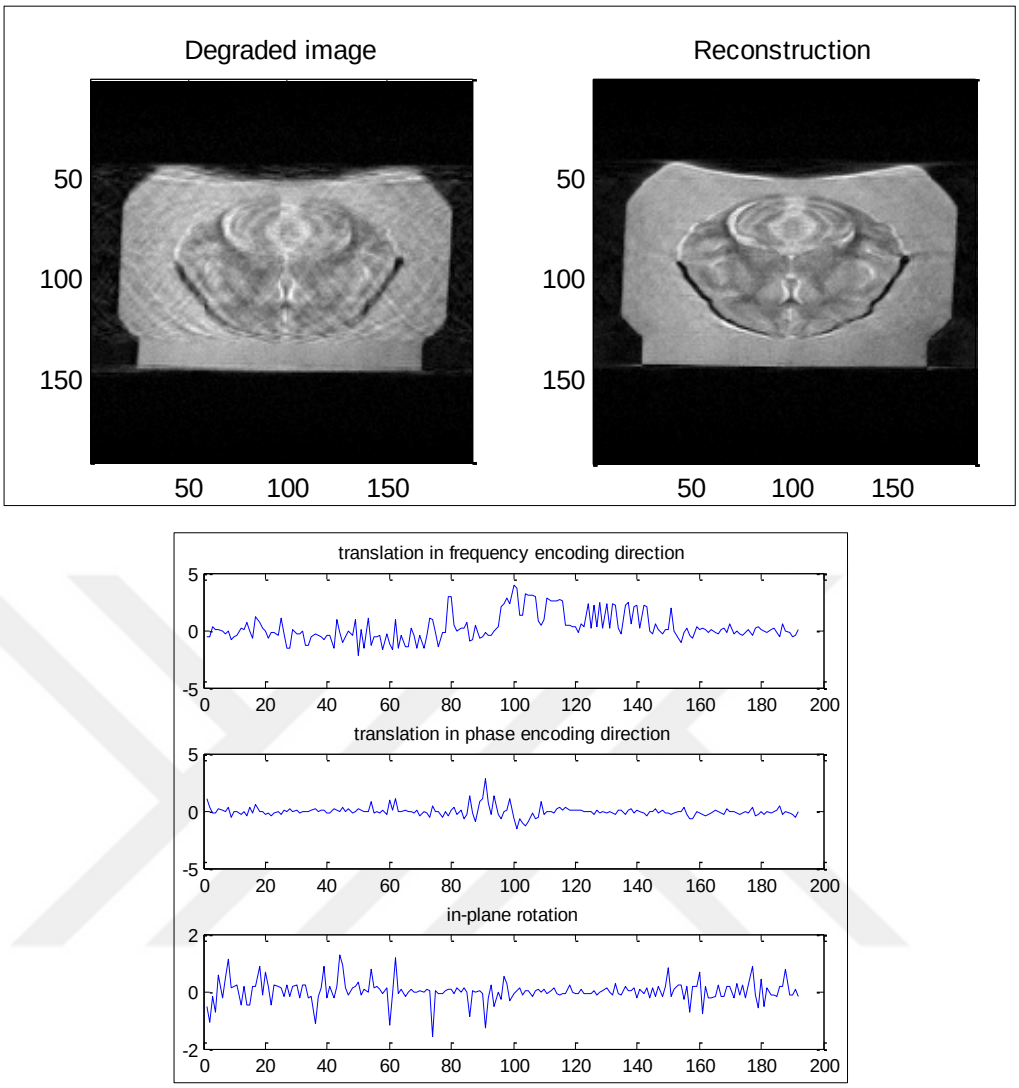

Figure 5.5 Monkey brain image with 2D dimension (raw data 3). Left: degraded image of monkey brain. Right: corrected with using optimization of image quality metric over the raw data. The bottom chart, with random values launching three DOFs algorithm parameters are obtained in 2D: depends on the straight line trajectory shows a sinusoidal curve motion.

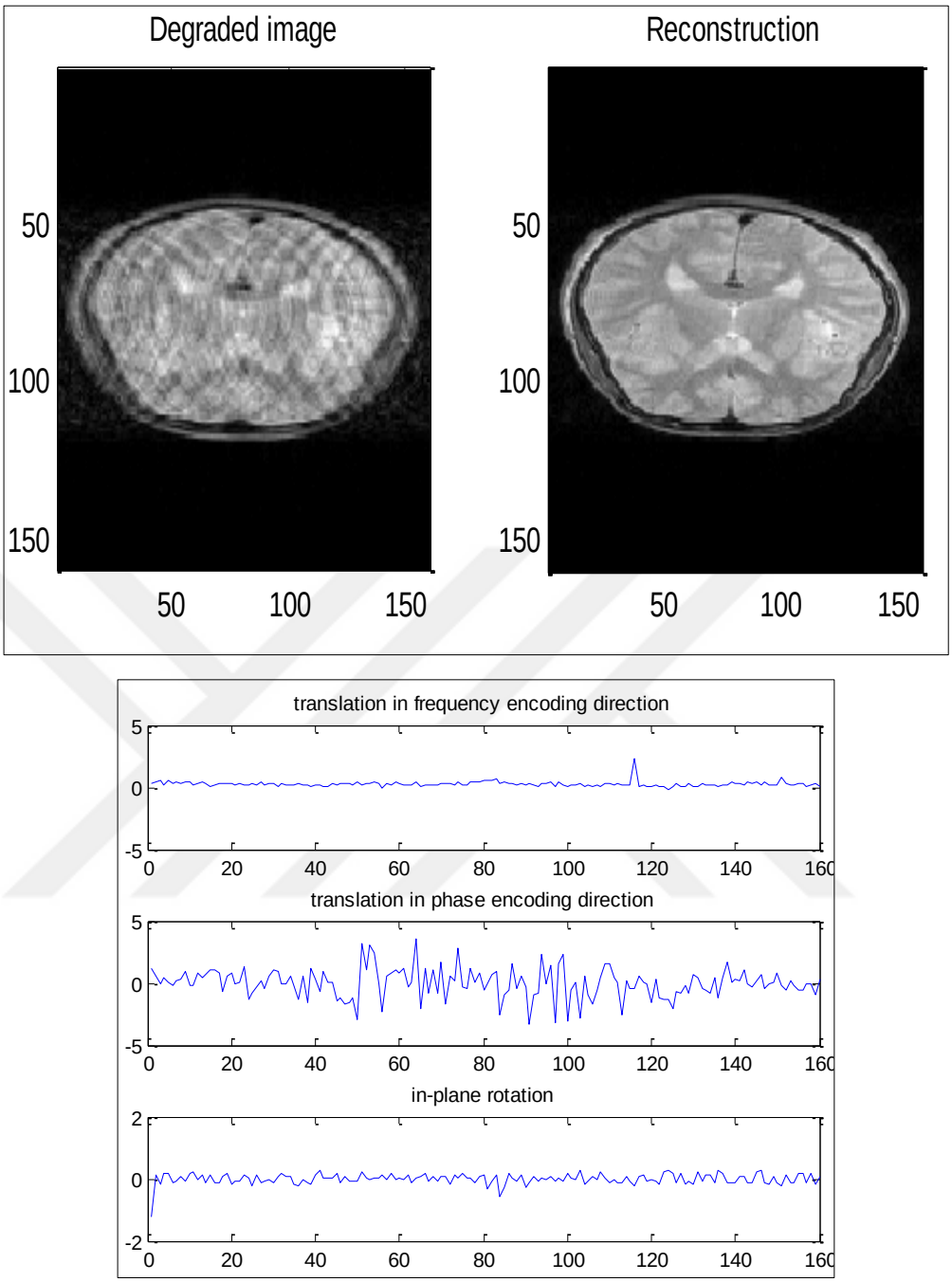

Figure 5.6Human brain image with 2D dimension (raw data 4). Left: degraded image of human brain. Right: corrected with using optimization of image quality metric over the raw data. The bottom chart, with random values launching three DOFs algorithm parameters are obtained in 2D: Depends on the straight line trajectory shows a sinusoidal curve motion.

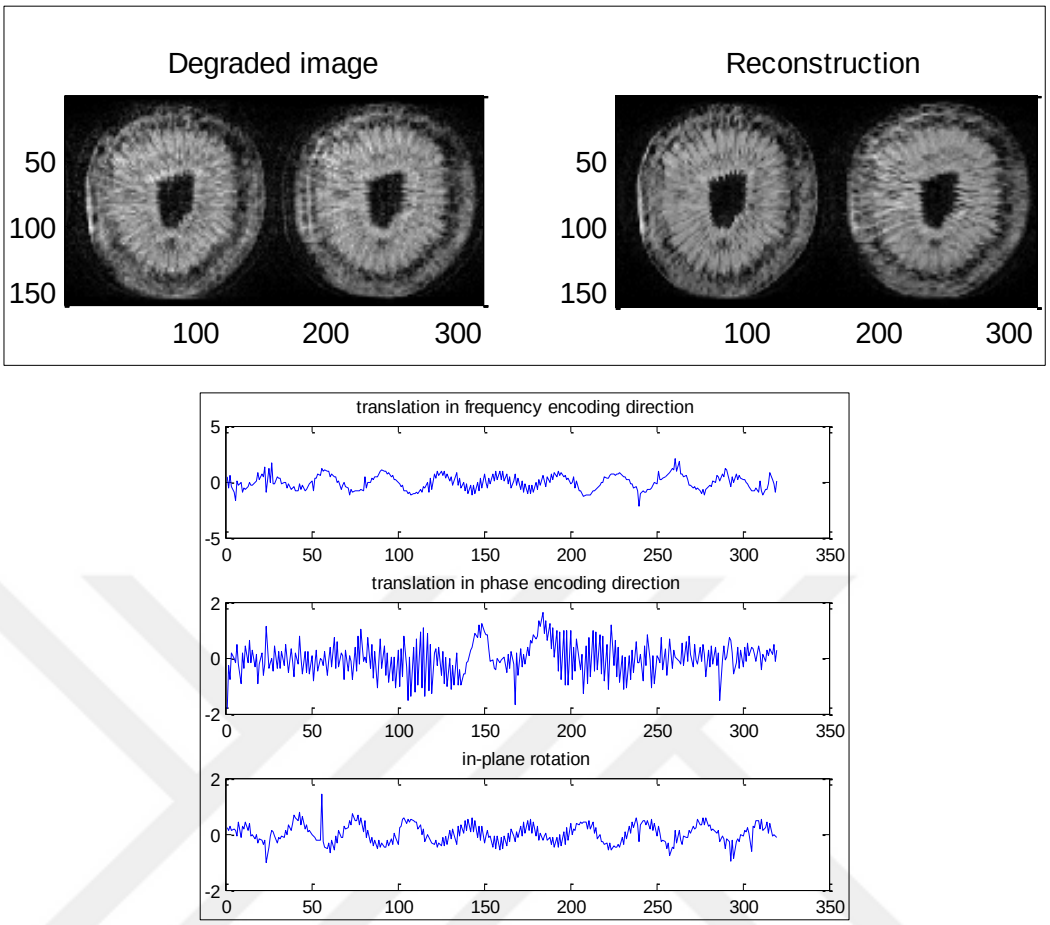

Figure 5.7 Motion correction application of data recorded by 3D FLASH sequences of 2D of kiwi fruit (raw data 5). Left: degraded image of kiwi fruit. Right: corrected with using optimization of image quality metric over the raw data. The bottom chart, with random values launching three DOFs algorithm parameters are obtained in 2D: Depends on the straight line trajectory shows a sinusoidal curve motion.

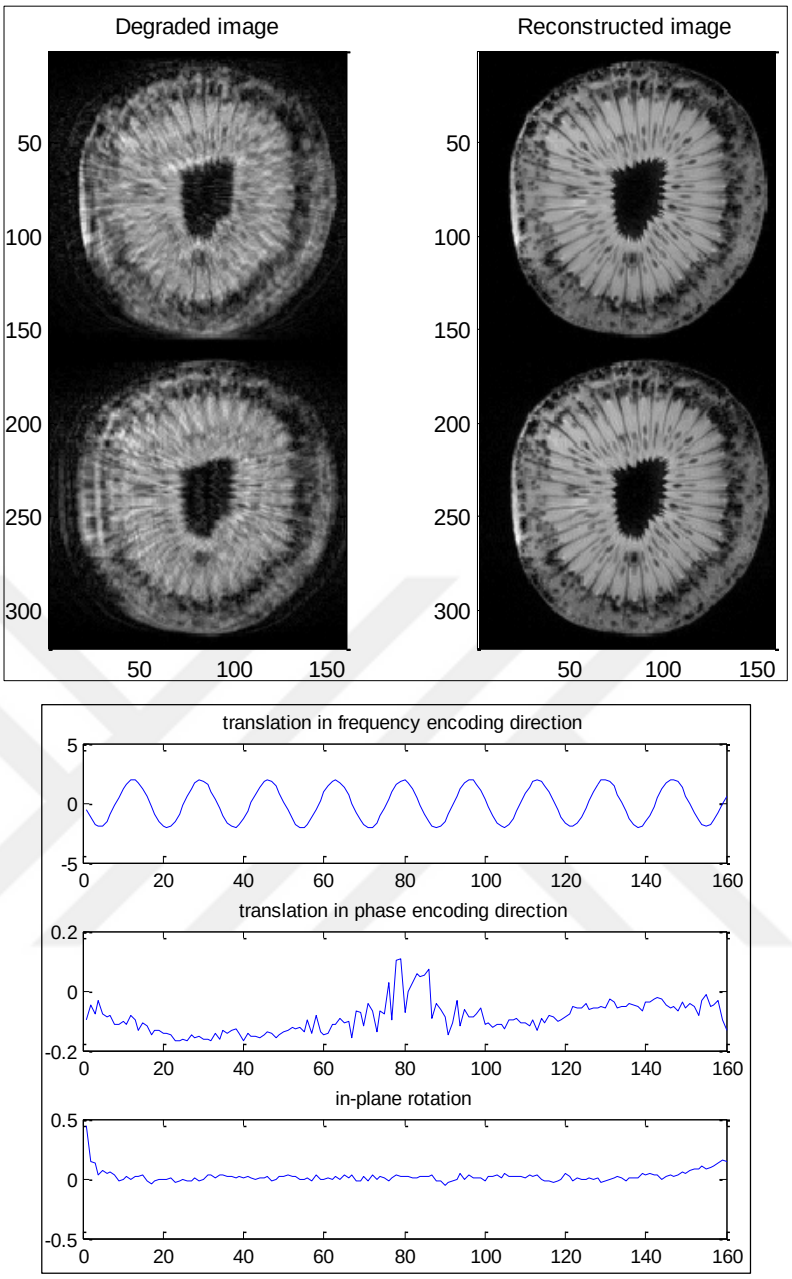

Figure 5.8 Motion correction application of data recorded by 2D FLASH sequences of 2D of kiwi fruit (raw data 6). Left: degraded image of kiwi fruit. Right: corrected with using optimization of image quality metric over the k-space. The bottom chart, with random values launching three DOFs algorithm parameters are obtained in 2D: depends on the straight line trajectory shows a sinusoidal curve motion.

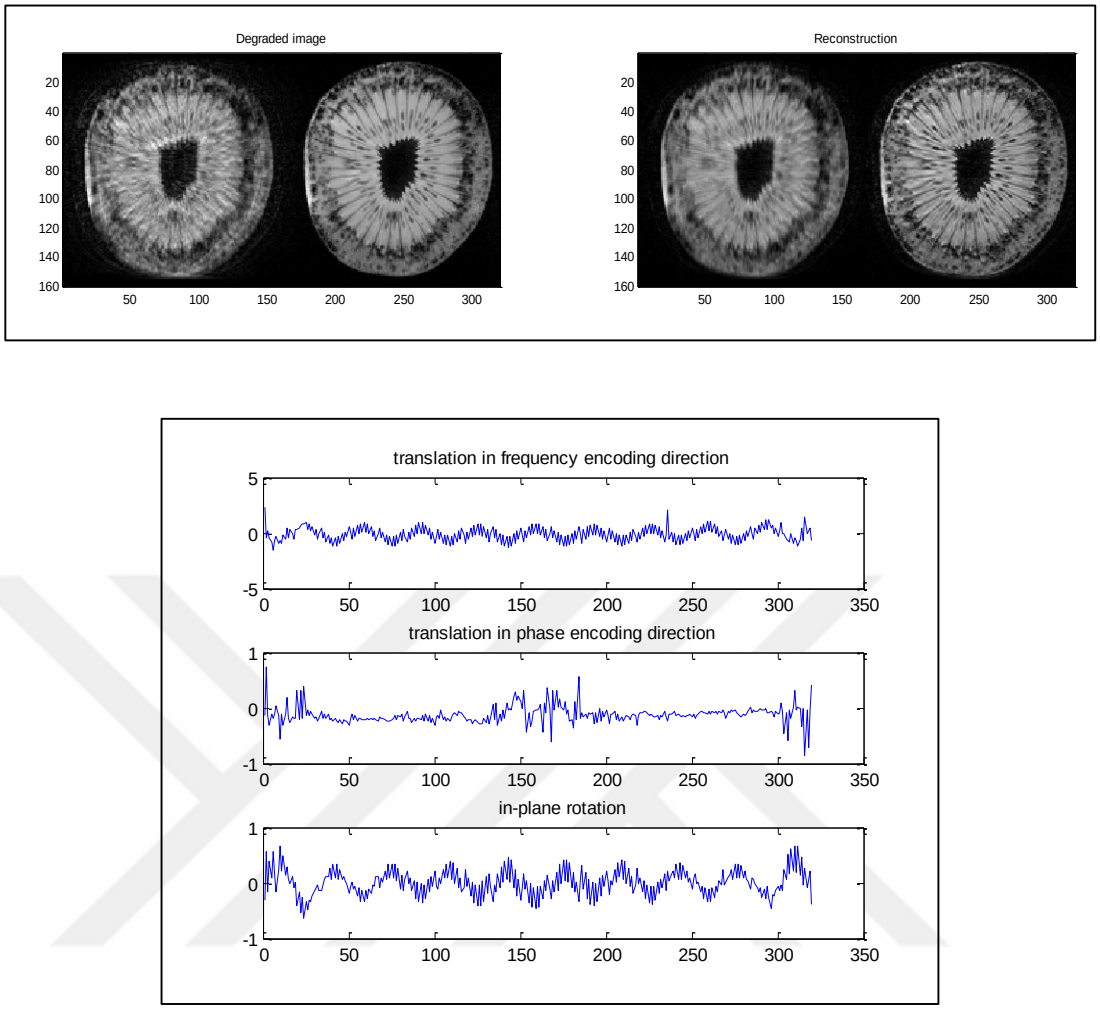

Figure 5.9 Motion correction application of data recorded by real data FLASH sequences of 2D of kiwi fruit (raw data 7). Left: degraded image of kiwi fruit. Right: corrected with using optimization of image quality metric over the raw data. The bottom chart, with random values launching three DOFs algorithm parameters are obtained in 2D: Depends on the straight line trajectory shows a sinusoidal curve motion.

Techniques based on prospective motion correction, one of the most important techniques in the recent years are depend on fuzzy entropy approach and obtained better results in this research. One of the reasons why the suggested technique is effective (general advantage of backward techniques) is that it is being practicable without any previously acquired data. It is an advantage in terms of cost that any monitoring equipment or special monitoring techniques are not required. These techniques can be widened for non-rigid body motion by practising additional restrictions (Se Young, 2009).

By using gradient based optimization techniques, motion parameters are found in MR scanning's which include motion artifact and problems of non-linearity, large dimensionality and long calculations due to optimization are solved. For AF approaches used before is acquired by translation or rotation practices of motion parameters in k-space and metric image quality measurement techniques are used for finding the best parameter for every image (Sungheon et al., 2008). As the suggested methods in this study are inefficient for motion artifact with a rotation bigger than 4°, we tried to keep our practices with 4°. However, the image after practices is not worse than the image whose quality is distorted.

Accurate renewable experimental results cannot be obtained due to significant data loss occurred in k-space as a result of heavy rotation (angles larger than 4°). As an alternative, new heavy parameters can be predicted by minimizing with the suggested technique in which the difference between estimation of motion parameters and sharp image parameters are used (Wenda et al., 2005). Fuzzy entropy based conjugate gradient method used for motion artifact correction in MRI. (Srinivasa et al., 2012).

It is seen that convergence problems occur when artifact corruption is made with the alternatives given briefly above. In the process of the last image, the reciprocal can be taken with an alternative mathematical technique by using empirical inversion technique. In related experiments, the results acquired from taking the reciprocal are not compared with experimental reversibility in terms of taking better accuracy results.

The comparison of conjugate gradient based on fuzzy entropy technique with the others and the evaluation of the results will be explained with examples. Forward model will be used for creating bad data with a 2D image including freedom of movement on stimulations (Wenda et al., 2005). The comparison of trajectories having motion distortion acquired from reconstruction algorithm with real reference ones will be practiced with this technique (Pipe, 2000). It helps to compare motion trajectory. Both rotation and translation motion is simulated in this research. For each motion parameter, the motion trajectory is acquired as a sinusoidal form (see the image 4). Sinus form which describes motion distortion on the whole image is compared in all

figures with the sinus form describing reference values. As it is seen in figures, parameters have a value between -4° and 4° and translation parameters take value between -5 and 5. In which trajectory has more rotation or translation can be seen through the centre of k-space as it is in sinus-form. In the images where motion artifactis low; for example in figure 8, motion distortion is less than in the graphics given in sinus-form.

For the 2D image of the brain given in Figure 5.8 (matrix size N = 192 × 192). Degree of freedom (DoF) in the form of out-of-phase sinus data will be acquired by a patient which is moved synchronously or stimulated. Optimum estimators whose initial value is chosen randomly are obtained in sinus-form in 100 successful consecutive tests. As it is seen in the other images, correction of motion artifact is also visually successful clinically. In addition to visual clarity, successful results are obtained comparing to literature in terms of image quality metrical measure which is used for image processing. It is accepted as successful comparing before the process according to criteria of NRMSE (normalized root mean square error), SNR (signal to noise ratio) and DBE (difference in background energy) which are the most common ones in literature.

When bad data acquired from trajectories are evaluated in accordance with reference values, it is seen that the bad data occurs due to not existence of high and medium frequencies in the centre of k-space. However, this contradiction is seen in the areas near DC (DC component is the centre of abscissa). The reason of this is the areas are not affected by motion distortions as DC value is high in the centre of k-space. It is totally stable to k-space and it is not sensible to the motion because restoring probably does not distort the image. Iteration is not made until optimal motion parameters are not obtained by motion parameters initiated with zero for restoration.

The standard deviation (SD) and mean of rotation, translation parameters and other quality metric are given in Table 5.1. Value of standard deviation of rotation parameters are quite high data 2 and data5 in Figure 5.10. These differences significantly affect the corruption seen in the picture. When translation parameters are

observed in Figure 5.11, the value of standard deviation creates significant differences in data 2 and data5. The mean of translate coefficient in y direction generally is higher than the x direction as generally observed in Figure 5.12 and in Figure 5.13. Similarly, the value of standard deviation of translate coefficient in the y direction seems higher.

Table 5.1 Statistics of translation - rotation parameters and Quality metrics

Data(Image) no	SD rotation	SD translation	Mean rotation	Mean translation	DBE	1-NRMSE	SNR I_{art} / I_{corr}
1	0.2626	0.3053/0.3211	0.4111	0.5724/0.5740	0.4965	0.85	30/39
2	0.1171	0.2001/0.1236	0.2199	0.2787/0.1226	0.2956	0.80	20/22
3	0.2862	0.8931/0.3448	0.2949	0.8404/0.2768	0.4857	0.86	27/30
4	0.1171	0.2001/0.1236	0.2199	0.2787/0.1226	0.3547	0.93	36/42
5	0.1156	0.2083/0.7969	0.1264	0.2648/0.8761	0.4463	0.84	30/34
6	0.1953	0.3734/0.3694	0.2787	0.5596/0.4839	0.3552	0.81	24/28
7	0.1432	0.3649/0.1160	0.1770	0.5014/0.1643	0.2552	0.92	55/65

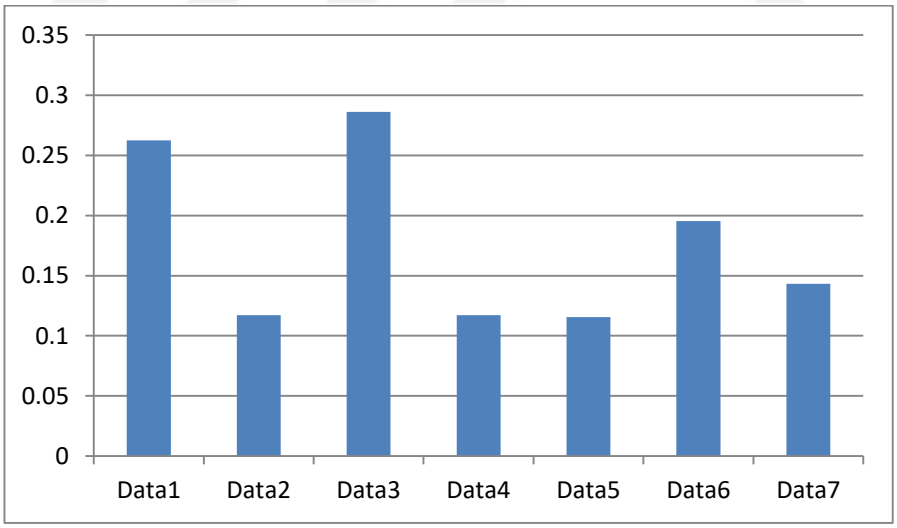

Figure 5.10 Standard deviation of rotation parameters

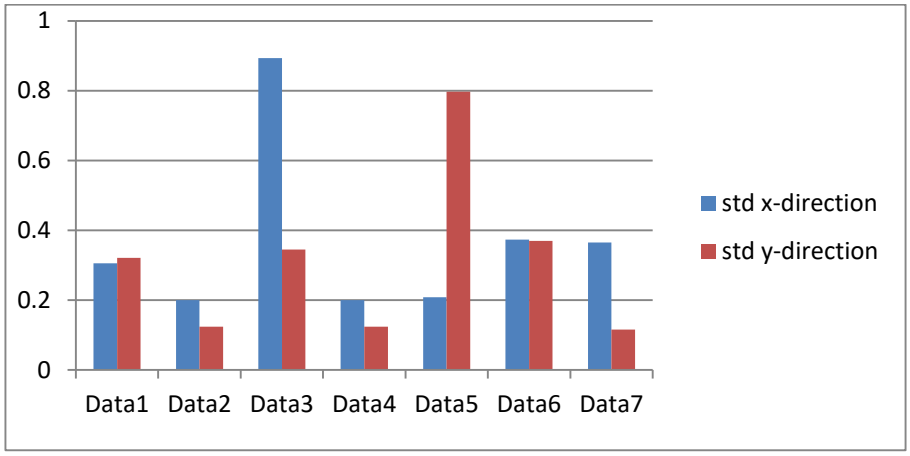

Figure 5.11Standard deviation of translation parameters for y- direction and x- direction

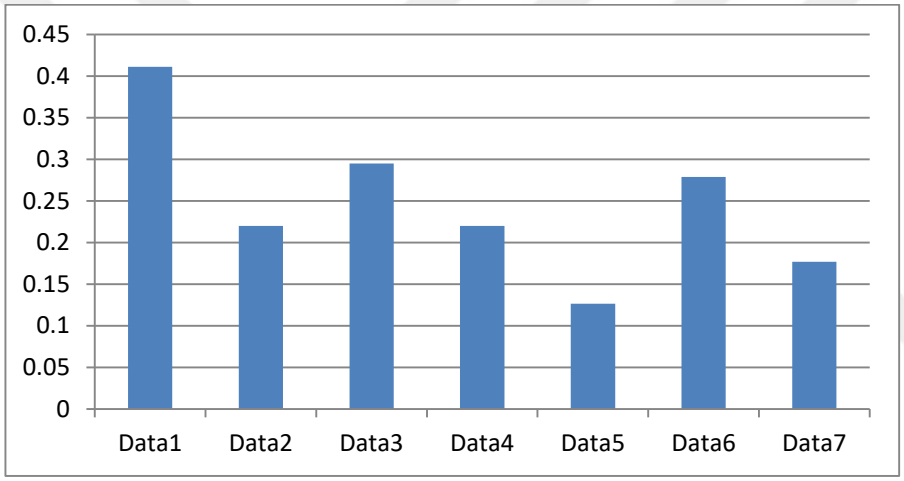

Figure 5.12- Mean of rotation parameters of all images

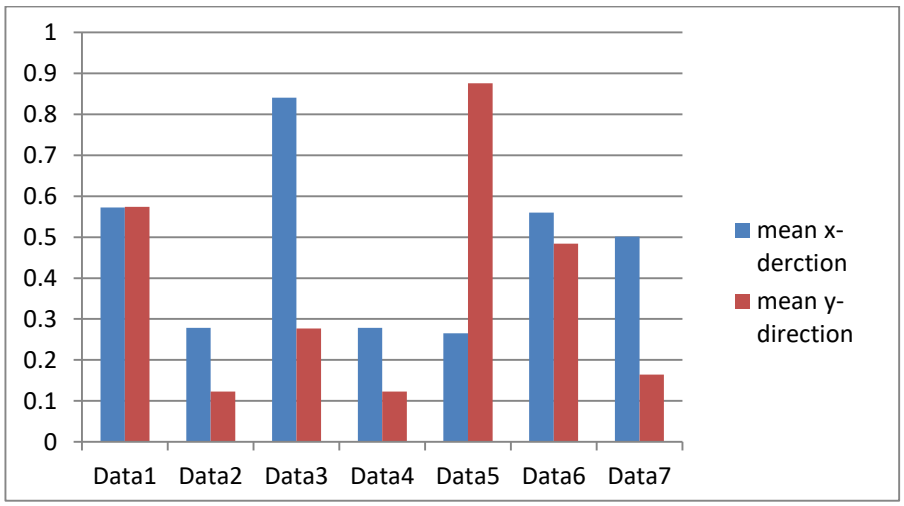

Figure 5.13 Mean of translation parameters for x- direction and y- direction

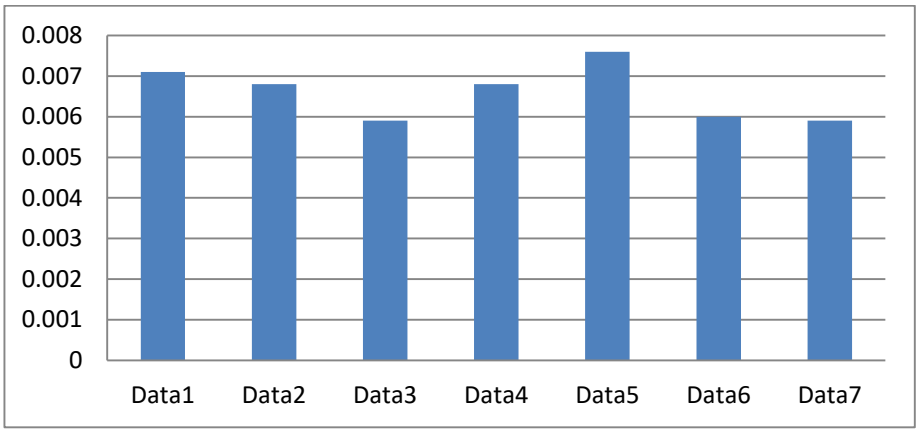

Figure 5.14 Mean of rotation parameters of original image

In order to eliminate artifact in image, the value of 1-NRMSE given in Figure 5.15 are the normalized results of the difference between the corrected image and distorted picture. As long as this value is nearer to 1 correction, an excellent success in correction is seen. As it can be seen from the pictures, data 2, data 4 and data 7 seems to be very successful in correction and obtained an over 84% correction according to the other images reputation. Bourgeois et al's articles which published in 2003, they found values of 1-NRMSE in the range of 75-90. In our study, these values were in the range of 84-93 (Bourgeois et al., 2003).

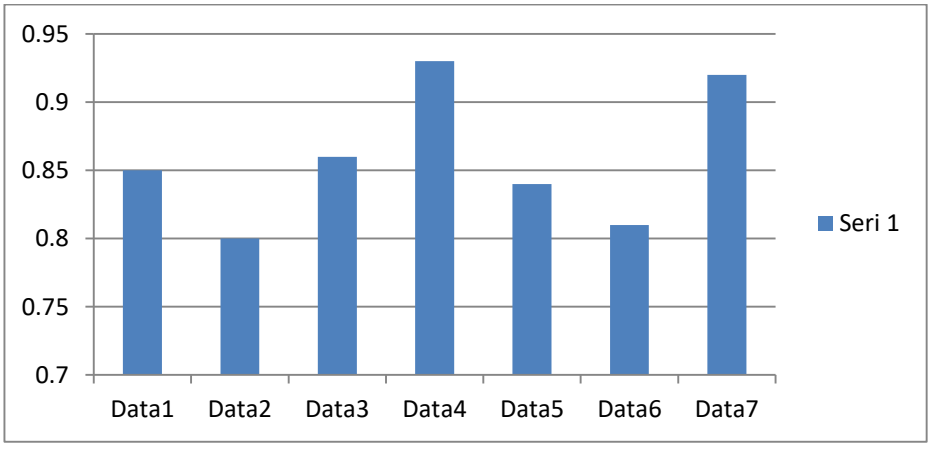

Figure 5.15 1-NRMSE value is different corrupted image and corrected image

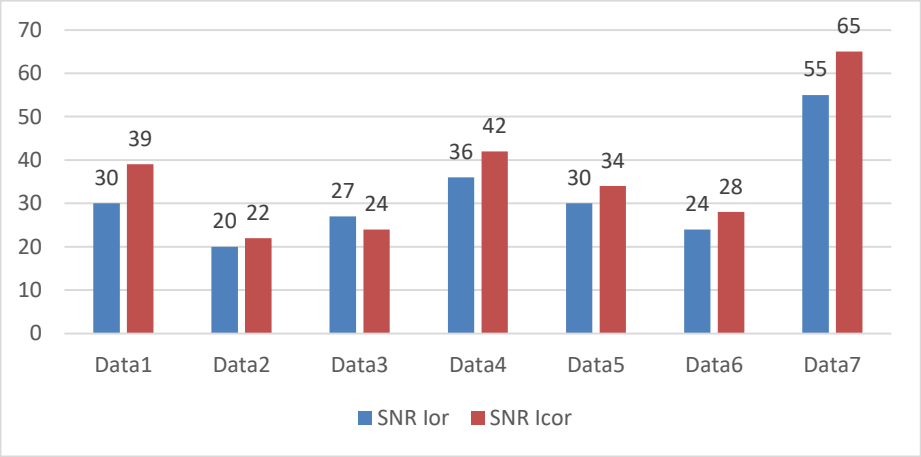

Figure 5.16 SNR of corrupted image and corrected image is different another. SNR value of corrected image higher than corrupted image

Other quality metrics that means the correcting success are SNR values. SNR values of the corrupted image appears to be quite low compared to the SNR of the corrected image. It also shows us that the success of the applied motion correction method is efficient on MRI technique. SNR of corrected images in our study, this value is approaching 180, while another most 100 in literature in Figure 5.16.

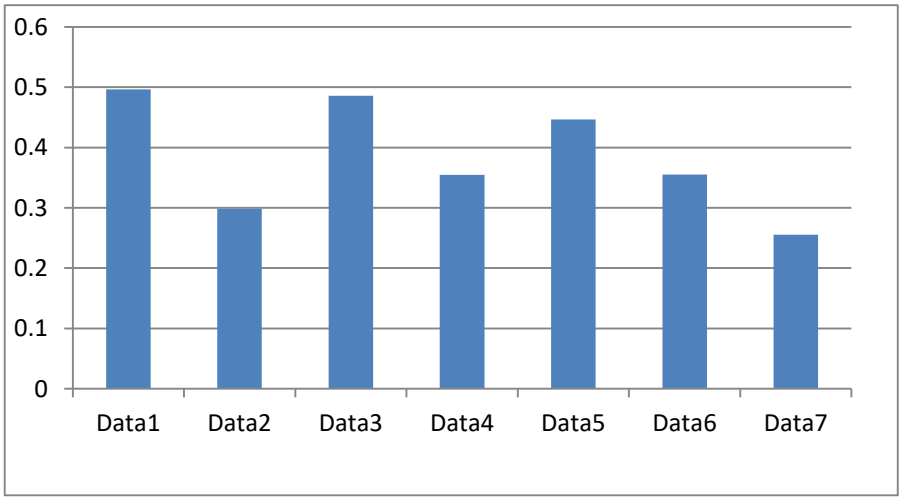

Figure 5.17 DBE ratio of background corrupted image and background corrected image

DBE values for images in are approaching 0.2552. These values confirm the order of image quality that is already apparent to the eye and quantifies the level of artifact in Figure 5.17. One of the image quality metric is DBE, which purposed a new measure of the MRI image and background noise. 1-DBE value represent ratio of motion

artifact reduction in final MRI image. DBE ratio of background corrupted image to background corrected image noise have value same as SNR value which given in Figure 5. 15.

At another stage of the study, 31 expert opinions are received in terms of evaluation of improvement in MR images. The evaluations made by 31 radiologists in the modelled images were examined. Each expert reviews the images with Corrupted image and Corrected image. The results of this evaluation were obtained by face-to-face interviewing by forming a form (Appendix-2) in which scores can be given between 1-10 points (1: Very bad 2: Bad ... 9: Good 10: Very good). Student t test is used for the analysis of the obtained results. Table 5.2 shows the average points and standard deviations for each image of the experts. All image evaluation scores are not normally distributed because $p < 0.05$ in in Table 5.2.

Table 5.2 Expert point averages and standard deviations

Data (Image) No	Mean	Std. Deviation
Data1	7.7742	0.66881
Data2	6.6452	1.64415
Data3	7.1935	1.30178
Data4	6.8065	2.22740
Data5	8.3548	1.17042
Data6	6.6774	1.49191
Data7	9.1290	0.61870

As seen in Table 5.3, it is seen that the average of the expert improvement points is higher than 6 ($p < 0.05$). We can say that it is statistically significant.

Table 5.3 One-Sample t Statistics

	Test Value = 6	
	t	Sig. (2-tailed)
Data1	14.770	.000
Data2	2.185	.037
Data3	5.105	.000
Data4	2.120	.042
Data5	11.202	.000
Data6	2.528	.017
Data7	28.158	.000

Expert point average and 1-NRMSE values are shown together in Figure 5.18. Here, it seems that they are quite similar to each other in two consequences.

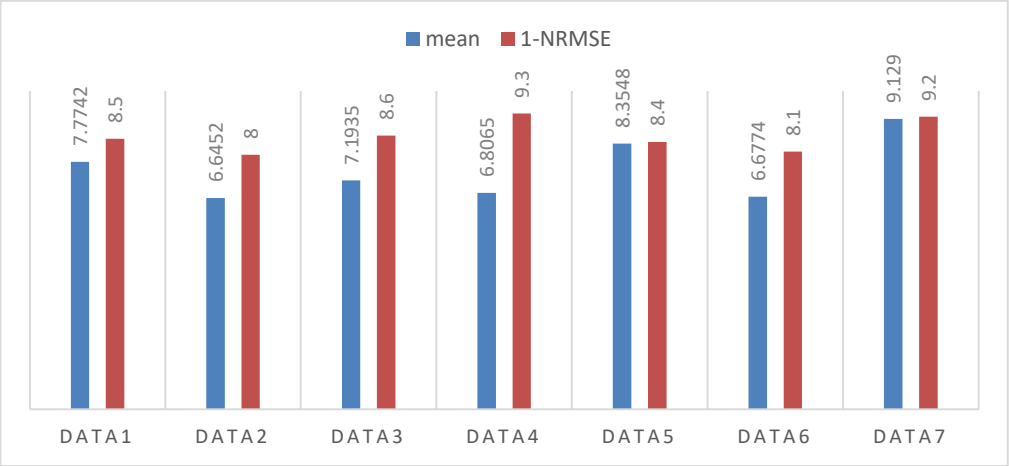

Figure 5.18 Expert point average (mean) compare with 1-NRMSE

Looking at the average scores of each picture given in Table 5.2, it is seen that the minimum Data2 is 6.6452. These results mean that the artifact in the images is reduced at least 67%. The results from radiologists' evaluations are very similar to other quality measures.

CHAPTER SIX
CONCLUSIONS AND FUTURE WORK

The aim of this thesis is to develop the process of getting a new MRI image algorithm to correct distortions caused by patient motion. A method which can estimate parameters pertinent with recommended Image reconstruction from the estimated sample position (reconstructing) and automatic motion correction. This method uses only k-space (raw data) data (Lauze et al., 2015). If we used a code to correct distortions arising from rotation and translation coarse to fine strategy and conjugate gradient methods based on fuzzy entropy, it was realized by arranging an optimal algorithm. In this study, it is proved that motion correction process performed on random sampling and the less sampled k-space is successful.

Conceptually, the 2D method can be extended as the process of data acquisition like 3D EPI-like. If the signal reading during patient's motion is ignored (short signal reading time), rotation will negatively affect the organization of the data in the k-space. In this case it seems to be that the translation phase encoding directions create encoding toward different directions. We don't need to know the sensitivity of the coils to make the motion correction (coil sensitivity). If the sensitivity of the coils is known, parameters of our proposed method this sensitivity. For example, motion distortions can be corrected by removing sensitivity mask from the combined mask (mask unity) with the opposite taking method. The mechanisms as a reason under this, is that high-density pixels are visible on profile areas outside coils. Because this parameter to predict the movement requires an appropriate inverse method applied to take some imaging processes such as parallel imaging.

In summary, we offer the prediction of the movement parameters by the fuzzy entropy based on conjugate gradient method and the retrospective method which has motion correction capability (Zahneisen et al., 2016). We have developed an analytical coarse to fine-based model to estimate the motion parameters on high-dimensional matrix space formed with our cost function gradient (Nan-Kuei & Alice, 2004). The success of the proposed method can be observed by the executed applications using

raw data which obtained from UMRAM in Bilkent University. Thus, irregular sampling results arising from movements on the 3D k-space and k-space of which curved linear trajectories consisting of bend lines is obtained in 2D space. The motion parameters have been estimated by using three parameters (two for translation and one for rotation) for each trajectory. All simulations were performed using the algorithm developed in MATLAB programming. In our later study, six motion parameters (three for translation and three for rotation) will be estimated by enlarging the method used in 2D space for 3D space.

This method which does not require additional equipment and software can be applied to MRI devices having different sequences properties. The fuzzy entropy approach is especially recommended in the literature to find optimal solutions. Successful results have been reached by adapting fuzzy entropy approach to conjugate gradient method in estimating parameters. The resulting obtained effective results compared to the similar studies in terms of metrics quality. 1-NRMSE based on mean squared error value is calculated as from 85 to 97 that is the proposed method reaching from 85% to 97% succeed. SNR of corrected images in our study approaches 65, while most in literature are 60. For example, the articles by Bourgeois, et al, which were published in 2003, they found values of 1-NRMSE in the range of 75-90. Seddeq et al was found values of SNR in the range of 10-30 and values of 1-NRMSE in the range of 60-80 in 2010. DBA as a new quality metric result shows that removal of motion artifact problems are over than 70% (Seddeq & Salahaddin, 2012).

REFERENCES

Abaci, E., Ider, Y. Z., & Atalar, E. (2015). Approximate Fourier domain expression for Bloch–Siegert Shift. *Magnetic Resonance in Medicine, 73*, 117–125.

Ahunbay E. & Pipe, J. G. (2000). Rapid method for deblurring spiral MR images. *Magnetic Resonance in Medicine*, *44*(3), 491–494.

Alexander, S.L., & Yablonskiy, D. A. (2003). Gaussian approximation in the theory of MR signal formation in the presence of structure-specific magnetic field inhomogeneities. *Journal of Magnetic Resonance*, *163*, 236–247.

Allison, J. M. (2016). *Regularized MRI Coil sensitivity estimation using augmented lagrangian methods.* Ph.D. Thesis, University of Michigan, USA.

Alonso, B. & Massiot, D. (2003). Multi-scale NMR characterisation of meso structured materials using 1H- 13C through-bond polarisation transfer, fast MAS, and 1H spin diffusion. *Journal of Magnetic Resonance*, *163*, 347–352.

Amy, K., Robert, G., Paden, A. C. , Silva, J. ,L., Kujak H., J. & Lawder, W .(2009). Iterative reconstruction technique for reducing body radiation dose at CT: Feasibility Study. *American Roentgen Ray Society*, *193*, 764–771.

Angelina, P., Karen, T., Paul, B. & Nancy, L. (2012). Phantom study of the impact of adaptive statistical iterative reconstruction on image quality for paediatrics computed tomography. *Journal of Biomedical Science and Engineering*, *5*, 793-806.

Bertram, R., Asbury, T. , Fabiola, F. , Quine, J.R. , Cross, T.A. & Chapman, M.S. (2003). Atomic refinement with correlated solid-state NMR restraints. *Journal of Magnetic Resonance*, *163*, 300–309.

Bourgeois, M.E., Wajer, F.T., Roth, M., Briguet, A., Décorps, M., Ormondt, D., Et al. (2003). Retrospective intra-scan motion correction. *Journal of Magnetic Resonance, 163*, 277–287.

Callaghan, Martina F. Josephs, O., Herbst, M., Zaitsev, M., Todd, N., & Weiskopf, N. (2015). An evaluation of prospective motion correction (PMC) for high resolution quantitative MRI. *Frontiers in Neuroscience*, *9*, 277–288.

Chaumette, H., Grandclaude, D., & Canet, D. (2003). Rotating-frame spin–lattice relaxation time imaging by audio-frequency field gradients: visualization of strained cross linked natural rubbers. *Journal of Magnetic Resonance*, *163*, 369–373.

De Luca, A. & Termini, S. (1988). Entropy measures in fuzzy set theory. *Systems and Control Encyclopedia*, 1467-1473.

Duer, M.J. (2002). *Solid State NMR Spectroscopy: Principles and applications*. USA: Blackwell Science Ltd..

Dung, T., Truong, Q., Sehoon, Y., & Anthony, V. (2009). Adaptive fuzzy filtering for artifact reduction in compressed images and videos. *IEEE Transactions on Image Processing*, *18*(6), 1166-1178.

Ernst, M., Samoson, A., & Beat Meier, H. (2003). Low-power XiX decoupling in MAS NMR experiments. *Journal of Magnetic Resonance*, 163, 332–333.

Fagan, A. J., Davies, R. G., Hutchison, J. M., Glasser, F. P., & Lurie, D. J. (2003). Continuous wave MRI of heterogeneous materials. *Journal of Magnetic Resonance, 163*, 318–324.

Fatemi, A. (2011). Entropy of stochastic intuitionistic fuzzy sets. *Journal of Applied Sciences, 11*(4), 784-751.

Fellner, C., Menzel, C., Fellner, F.A., Ginthoer, C., Zorger, N., Schreyer, A., Jung, E.M. & Feuerbach, S. (2010). BLADE in sagittal t2-weighted mr imaging of the cervical. *American Journal of Neuroradiology*,*31*,674–81.

Flemming, H. D., & Led, J. J. (2003). Implications of using approximate Bloch–McConnell equations in NMR analyses of chemically exchanging systems: application to the electron self-exchange of plastocyanin. *Journal of Magnetic Resonance, 163*, 215-227.

Forkert, N.D., Richberg, S.A., Fiehler, J. Illies, T., Möller, D., Handels, H. & Säring, D. (2011). Fuzzy-based Vascular Structure Enhancement in Time-of-Flight MRA Images for Improved Segmentation. *Methods of information in medicine*, *50, 74-83.*

Gonzales, R. C. & Woods, R. E. (2008). *Digital Images Processing*. USA: Prentical Hall.

Hinge-Chiu, C., Tzu-Chao, C., Yi-Ru, L., Fu-Nien, W. & Teng-Y. (2013). Correction of geometric distortion in propeller echo planar imaging using a modified reversed gradient approach. *Quantum Imaging Medicine Surgery*, *3*(2), 73-81.

Jackson, J. I., Nishimura, D. G., & Macovski, A. (1992). Twisting radial lines with application to robust magnetic resonance imaging of irregular flow. *Magnetic Resonance in Medicine, 25*(1), 128–139.

James, G. (1999). Motion correction with propeller MRI: application to head motion and free-breathing cardiac imaging**.** *Magnetic Resonance in Medicine, 42*, 963–969.

Julian, R.M. (2008). *Motion detection and correction in magnetic resonance imaging*. Ph.D. Thesis, University of Canterbury Christchurch, New Zealand.

Julian, R. M., Philip J., Bones, R.P. & Millane, R. (2008). MRI with TRELLIS: a novel approach to motion correction. *Magnetic Resonance Imaging, 26*, 474–483.

Kim, S., Dougherty, L., Rosen, M. A., Song, H. K., & Poptani, H. (2008). Automatic correction of in-plane bulk motion artifacts in self-navigated radial MRI. *Magnetic Resonance Imaging*, *26*, 367–378.

Kirsten P., N., James, G., Roger, B., & Joseph, E. (2001). PROPELLER MRI: Clinical testing of a novel technique for quantification and compensation of head motion. *Journal of Magnetic Resonance Imaging*, *14*, 215–222.

Klir, G. J. & Yuan, B. (1995). *Fuzzy sets and fuzzy logic theory and applications*. New Jersey: Prentice Hall.

Knutsson, H. Andersson, M., Borgay, L.(2016). *Respiratory artifact reduction in MRI using dynamic deformation modelling.* Retrieved May 23, 2016 from http://www.ami.imt.liu.se.

Kosko, B. (1994). *Fuzzy Thinking: The new science of fuzzy logic.* Flamingo Prentical Hall.

Kwan, Y. M. & Kwan, K. H. (2011). Impulse noise reduction in brain magnetic resonance imaging using fuzzy filters. *Journal of Medical, Health, Biomedical, Bioengineering and Pharmaceutical Engineering*, *5*(12), 688-691.

Koharudin, I., Leonardus, M., Alexandre, M.J., Bonvin, J., Kaptein, R., & Boelens, R. (2003). Use of very long-distance NOEs in a fully deuterated protein: an approach for rapid protein fold determination. *Journal of Magnetic Resonance*, *163*, 228–235.

Lauze, P., Estimation, F. & Kornprobst, E. (2015). *A coarse to fine multiscale approach for linear least squares optical flow*. Retrieved may *24*, 2015 from, www.irisa.fr/vista/Papers/2004_bmvc_lauze.pdf.

Madhu, P.K., Johannessen, O. G., Pike, K. J., Ray, Dupree, Smith, M. E., & Levitt, M. H. (2003). Application of amplitude-modulated radiofrequency fields to the magic-angle spinning NMR of spin-7. *Journal of Magnetic Resonance, 163,* 310–317.

Mesleh, M.F., Opella, S. J. (2003). Dipolar Waves as NMR maps of helices in proteins. *Journal of Magnetic Resonance, 163*(2), 288–299.

Michael, J. (2015). *Regularızed MRI Coıl sensitıvity estimatıon usıng augmented lagrange methods.* Ph.D. Thesis, University of Michigan, USA.

Michael, F. Keith, J. & Slifer, L. (2002). Operant-contıngency-based preparatıon of chıldren for functıonal magnetıc resonance ımagıng. *Journal of Applıed Behaviour Analysıs*, 35**,** 191–194.

Nan-kuei, C. & Alice, M. (2004). Removal of epi nyquist ghost artifacts with two-dimensional phase correction. *Magnetic Resonance in Medicine, 51,* 1247–1253.

Nasibov, E. N. (2008). A robust algorithm for solution of the fuzzy clustering problem on the basis of the fuzzy joint point's method. *Cybernetics and Systems Analysis, 44* (1), 7–17.

Pandey, K., & Noll, D. (2006). Improved activation detection in fMRI studies using acquisition and reconstruction methods robust to susceptibility and motion artifacts. *Magnetic Resonance in Medicine,* Seattle, *48*(5), 860–866.

Pandit, P., Qi, Y., Story, J., Kevin, F. & Allan J.G. (2010). Multi-shot PROPELLER for high-field pre-clinical MRI. *Magnetic Resonance in Medicine, 64*(1), 47–53.

Peder, E.Z., Michael, S. & Dwight G. (2008). Anisotropic field-of-view shape DOI: 10.1016/j.mri.2008.07.023 s for improved PROPELLER. *Magnetic Resonance Imaging*, *27*(4), 470-479.

Pipe, J. G. (1999). An optimized center-out k-space trajectory for multishot MRI: comparison with spiral and projection reconstruction. *Magnetic Resonance in Medicine*, *42*(4), 714–720.

Pipe, J. G. (2000). Motion Correction with PROPELLER MRI: Application to Head Motion and Free-Breathing Cardiac Imaging. *Magnetic Resonance in Medicine*, *42*, 963–969.

Pipe, J. G., & Ahunbay, E. (2000). Effects of interleaf order for spiral MRI of dynamic processes. *Magnetic Resonance in Medicine*, *41*(2), 417–422.

Pushpa, D. P., Vijay Kumar, T., & Sadhna, M. (2015). A novel fuzzy ımage enhancement using s-shaped membership function. *International Journal of Computer Science and Information Technologies, 6* (1), 564-569.

Ravindranathan, S., Mallet, J.-M., Sinay, P., & Bodenhausen, G. (2003). Transferred cross-relaxation and cross-correlation in NMR: Effects of intermediate exchange on the determination of the conformation of bound ligands. *Journal of Magnetic Resonance, 163*,199–207.

Reeder, B. S., Atalar, E., D. Bolster, B., & Elliot, R. (1997). Quantification and reduction of ghosting artifacts in interleaved echo-planar imaging. *Magnetic Resonance Medicine, 38*(3), 429–439.

Ryu Y., Choi Y., Cheon J., Ha S. & Kim W. (2016). Knowledge-based iterative model reconstruction: comparative image quality and radiation dose with a pediatric computed tomography phantom. *Pediatric Radiology*, *46*(3):303-15.

Sarty, G. E. (2000). Critical sampling in ROSE scanning. *Magnetic Resonance in Medicine*, *44*(1), 129–136.

Seddeq. E.G. & Salahaddin. M.S. (2012). Quality Evaluation of Compressed MRI Medical Images for Telemedicine Applications, *Biomedical, Bioengineering and Pharmaceutical Engineering*, *6*(12).

Scott, A. D., Keegan, J. & Firmin, D. (2009). Motion in Cardiovascular MR Imaging. RSNA Radiology. *250*(2).

Se Young C. (2009). *Motion aspects in joint image reconstruction and nonrigid motion estimation a dissertation.* Ph.D. Thesis, University of Michigan, USA.

Shu, Y. H., Riederer, S. J., & Bernstein, M. A. (2006). Three-dimensional MRI with an under sampled spherical shells trajectory. *Magnetic Resonance in Medicine, 56*(3), 553–562.

Slifer, K. J., Cataldo, M. F., Cataldo, M. D., Llorente, A. M. & Gerson, A. C. (1993). Behavior analysis of motion control for pediatric neuroimaging. *Journal of Applied Behavior Analysis*, *26*(4), 469–470.

Srinivasa, R. D., Seetha, M., & Krishna, P. (2012). Quality assessment of pıxel-level image fusıon usıng fuzzy logıc. *International Journal on Soft Computing* (IJSC), 3, 1.

Sungheon, K., Lawrence D., Mark Rosen, A., Hee Kwon, S. & Harish, P.(2008). Automatic correction of in-plane bulk motion artifacts in self-navigated radial MRI. *Magnetic Resonance Imaging 26*, 367–378.

Thomas, M. (2011). *Biomedical image processing biological and medical physics*. New York: Heidelberg Dordrecht.

Verdier, L., Sakhaii, P., Zweckstetter, M., & Griesinger, C. (2003). Measurement of long range HC couplings in natural products in orienting media: a tool for structure elucidation of natural products. *Journal of Magnetic Resonance, 163*, 353–359.

Wang, Fu-N., Huang, Teng-Y., Lin, Fa-H., Tzu-Chao C., Chen, Nan-K. (2005). Propeller epı: an MRI technique suitable for diffusion tensor ımaging at high field strength with reduced geometric distortions. *Magnetic Resonance Medicine*, *54*(5), 1232–1240.

Wenda. Z., Zhijun, X. &Jian, Z. (2005). Gradient entropy metric and p-Laplace diffusion constraint-based algorithm for noisy multispectral image fusion. *Information Fusion*, *27*, 138–149.

Yager, R.R., (1995). Measures of entropy and fuzziness related to aggregation operators. *Information Sciences*, *82*, 147-166.

Yingying, Z. & Connor, O., (2015). Fourier-based forward and back-projectors iterative fan-beam tomographic image reconstruction. *IEEE Transactions on Medical Imaging,* 25, 5

Yuusuke, H., Isoda, H., S. Maetani, Y., Arizono, S., Shimada, K., & Togashi, K. (2016). MRI artifact reduction and quality improvement in the upper abdomen with PROPELLER and prospective acquisition correction (PACE) technique. *Journal of Magnetic Resonance*, *163*,215–227.

Zadeh, L.A. (1965). Fuzzy Sets. *Information and Control*, *3*,338–353.

Zahneisen, B., Keating, B., Singh, A., Herbst, M. & Ernst, T. (2016). Reverse retrospective motion correction. Magnetic Resonance in Medicine, *75*(6), 2341–2349.

APPENDICES

APPENDIX-1

List of Abbreviations

Abbreviations used in this thesis are listed here for easy reference.

2DFT two-dimensional Fourier transform

CNR contrast-to-noise ratio

CT computed tomography

DBE difference in background energy

DFT discrete Fourier transform

DWI diffusion-weighted imaging

EPI echo planar imaging EPIC environment for pulse programming in

C FE frequency encode

FFT fast Fourier transform

FID free induction decay

fMRI functional magnetic resonance imaging

FOV field-of-view FSE fast spin echo GE General Electric (Medical Systems)

GRAPPA generalized autocalibrating partially parallel acquisitions GRASE gradient- and spin-echo

IEEE Institute of Electrical and Electronic Engineers

ISMRM International Society for Magnetic Resonance in Medicine MR magnetic resonance MRI magnetic resonance imaging

NRMSE normalized root mean squared error

NMR nuclear magnetic resonance

NMSE normalised mean squared error

PD proton density

PE phase encode

PET positron emission tomography

PROPELLER periodically rotated overlapping parallel lines with enhanced reconstruction

APPENDIX-2

MRI (Magnetic Resonance Imaging) Evaluation Form

Dear Expert,

In this study, a model was developed within the scope of doctorate thesis in DEU Institute of Science and Statistics. In the model, MRI row data from BILKENT University National Magnetic Resonance Research Institute (UMRAM) is used. There is movement artifact in row data. Artifact removal application was applied with the model created in the thesis study.

In this form, you are asked to evaluate clinically the success of correcting process within the range of 1-10 points (1: Very bad 2: Bad ... 9: Good 10: Very good) by looking at the Degraded image and Reconstruction image. Please circle your rating. After the scoring process, it is valuable for us to write down your comments, opinion and suggestions about the success of the method used on the evaluation form on the last page. We thank you for your contribution to our work.

Image 1

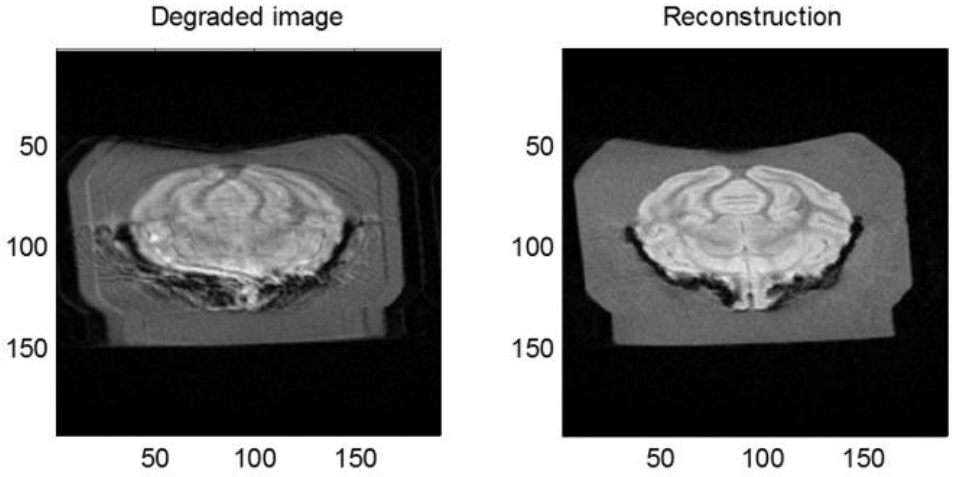

Degraded image **Reconstruction image**

Evaluation Score: **1 2 3 4 5 6 7 8 9 10**

Image 2

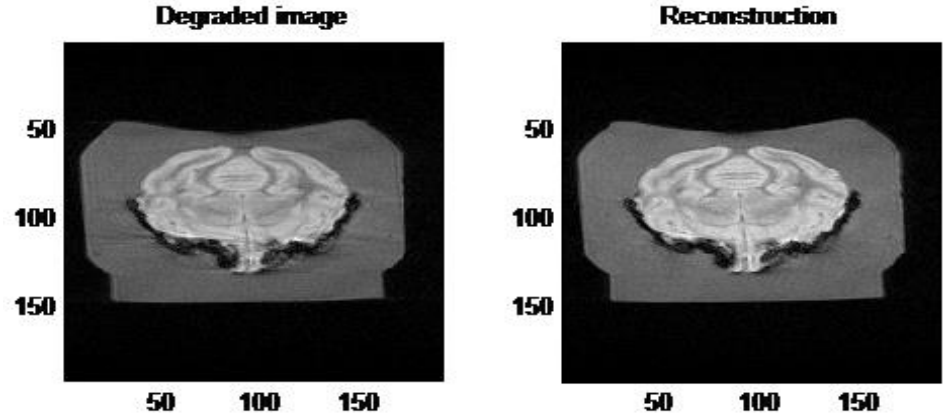

Degraded image **Reconstruction image**

Evaluation Score: **1 2 3 4 5 6 7 8 9 10**

Image 3

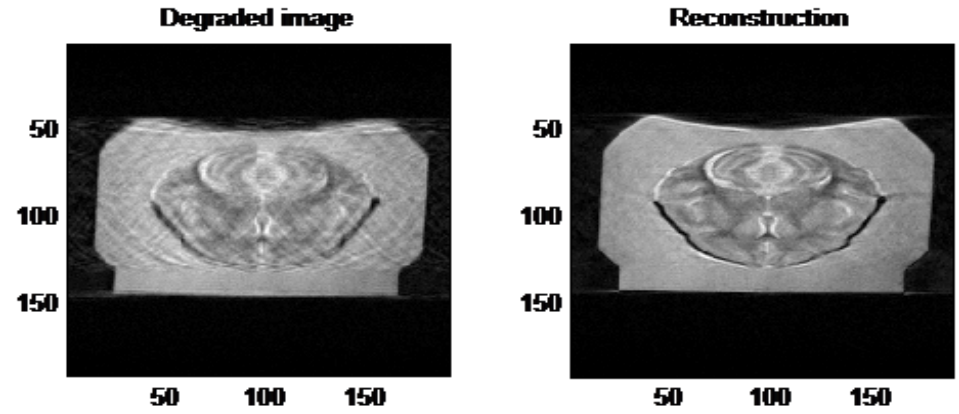

Degraded image **Reconstruction image**

Evaluation Score: **1 2 3 4 5 6 7 8 9 10**

Image 4

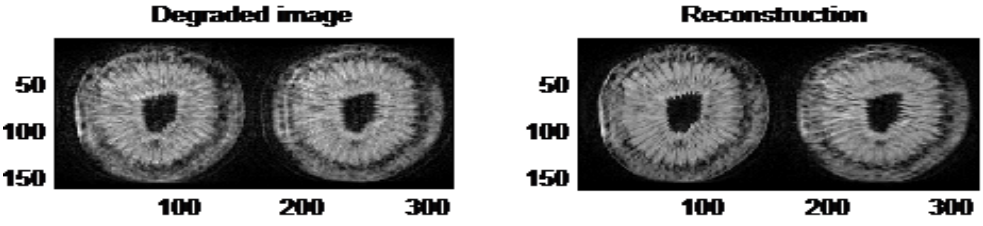

Degraded image **Reconstruction image**

Evaluation Score: **1 2 3 4 5 6 7 8 9 10**

Image 5

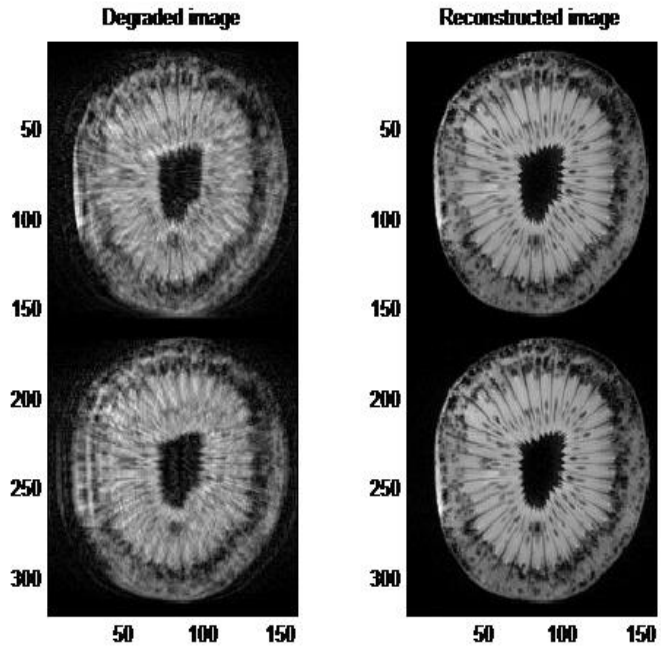

Degraded image **Reconstruction image**

Evaluation Score: **1 2 3 4 5 6 7 8 9 10**

Image 6

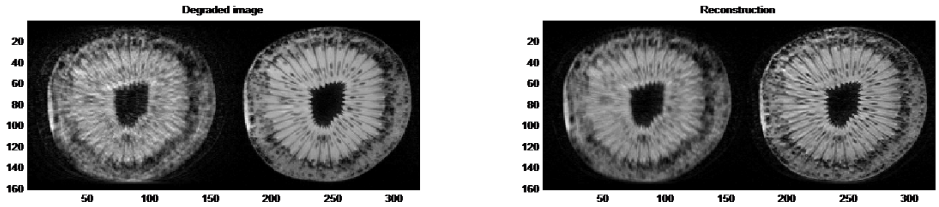

Degraded image **Reconstruction image**

Evaluation Score: **1 2 3 4 5 6 7 8 9 10**

Image 7

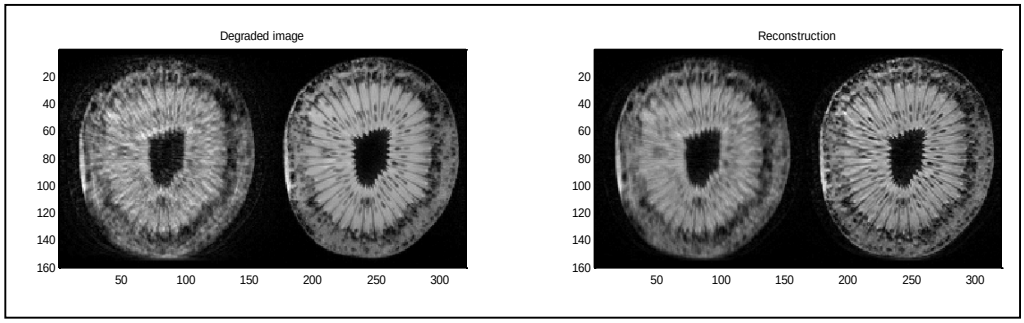

Degraded image **Reconstruction image**

Evaluation Score: **1 2 3 4 5 6 7 8 9 10**

Your opinions and suggestions:

……

……

……

……

……

……

……

……